

People's Democratic Republic of Algeria
Ministry of Higher Education and Scientific Research
University M'Hamed BOUGARA - Boumerdes -
Institute of Electrical and Electronic Engineering
Department of Electronics



Report Presented in Partial Fulfilment of the Requirement
of the Degree of

‘MAGISTER’

In **Electronics**

Option: **Telecommunication**

By

AÏCI Zakia

Title:

Data Fusion Processing In Brain Medical Imaging



Presented on 18th October 2011, before the jury

President:	M ^r BELOUHRANI Adel	Professor	ENP, Algiers
Members:	M ^{rs} OULEBSIR – BOUMGHAR Fatima	Professor	USTHB, Algiers
	M ^r DAHIMENE Abdelhakim	MCB	UMBB, Boumerdes
Supervisors:	M ^r BENTARZI Hamid	MCA	UMBB, Boumerdes
	M ^{rs} CHERIFI Dalila	MCB	UMBB, Boumerdes

Abstract

During recent years, medical imaging examinations more and more often use information acquired from multiple imaging modalities. This is mainly because the complementary information after fusion of the data, improves the quality of the diagnosis. For instance, the image fusion can be between data from different modalities or different individuals. It may also concern fusion of image data with an external model, which expresses prior knowledge about the problem at hand. Thus to have more information, medical image fusion is done which combines these complimentary features into one image. Generally it involves two steps, *registration* and *fusion*.

Registration deals with proper geometrical alignment of the images so that the corresponding pixels or regions of both images map to the same region being imaged. Registration is necessary in order to be able to compare or integrate the data obtained from different measurements. Therefore, correspondences between the two images are determined. Then, one image can be transformed into the coordinate system of the other. Perfect image registration is required to fuse the images.

Image Fusion essentially deals with the integration of information from different images to obtain a single image containing the complete information. In order to generate an overlapping image from different-modality images, image registration and various fusion techniques have been employed.

The objective of our work is to implement algorithms for fusing data on Medical images. For that, we have firstly developed registration methods which are: Rigid, Affine, Projective and Elastic. They are used to find a mapping or a transformation of points from one image to the corresponding points in another image. Secondly, we develop and implement Medical Fusion methods which use respectively logical operators, pseudocolormap, and clustering algorithms (k-means, fuzzy k-means, thresholding and EMsegmentation) for extracting and utilising information from several scans simultaneously in the analysis and diagnosis of patients. Finally, we applied the developed methods for different applications such as:

- Tumor's image extraction to monitor growth of tumor during a period of time,
- Extraction of normal tissue images and to add them to different modality to get one complete image.

Keywords: CT, MRI, Image registration, Image fusion, clustering algorithms, tumor identification, normal tissue recognition.

Résumé

Dans le cadre de traitement d'images et plus particulièrement le développement de méthode d'analyse d'images à des fins d'interprétation par des experts, le présent travail est orienté vers la fusion d'images médicales. L'objectif majeur et particulièrement dans le domaine médical, est l'aide à la compréhension et l'interprétation des images par les médecins. Afin que deux images puissent être correctement fusionnées, il faut les recalcr, c'est-à-dire déterminer les pixels ou régions, des deux images qui correspondent aux mêmes points ou aux mêmes régions. Le recalage est alors déterminant pour le processus de la fusion.

L'objectif principal de notre travail est de développer et implémenter des méthodes de recalage et de fusion appliquées aux images médicales cérébrales pour cela, nous avons abordé les techniques d'imagerie médicale, et mis l'accent dans cette étude, sur l'obtention d'images IRM et CT cérébrales. Puis, nous avons étudié et implémenté des méthodes de recalage spatial, et les outils mathématiques utilisés à savoir les transformations géométriques et les mesures de similarité.

Les méthodes de fusion permettent d'améliorer ou d'accroître la connaissance sur des points, des régions, ou des structures dans les images. Elles comportent deux étapes importantes à savoir le recalage d'image et la visualisation. Ces méthodes sont respectivement :

- Fusion Using Logical Operators
- Fusion Using a Pseudocolor Map
- Clustering Algorithms for Unsupervised Fusion of Registered Images
 - Kmeans Algorithm
 - Fuzzy Kmeans Algorithm
 - Threshold algorithm
 - Global threshold
 - Local Threshold
 - Otsu's algorithm
 - Brain classification based on EM segmentation

Une étude comparative entre les différentes méthodes implémentées sur des bases de données obtenues de différents centres d'imagerie médicales a été élaborée. Enfin, des applications ont été proposées tels que :

- La détection de tumeurs et suivie de l'évolution de tumeur sur des images IRM cérébrale.
- L'extraction de la structure d'une modalité d'image puis la fusionner avec une autre modalité.

Mots-clés: CT, IRM, le recalage d'images, la fusion d'images, les algorithmes de clustering, extraction de tumeur.

ملخص

تعدد طريقة تسجيل الصورة تلعب دورا متزايدا الأهمية في مجال الطب. الصور الطبية توفر معلومات أساسية عن التشخيص يمكن أن جودة الصورة تعطي معلومات المريض أكثر دقة، والتي يمكن استخدامها لتحسين عملية صنع القرار. يساعد الأطباء لاستخراج الميزات التي قد لا تكون مرئية عادة في الصور عن طريق طرائق مختلفة. وبالتالي لاستخراج مزيد من المعلومات، يتم دمج الصور الطبية في صورة واحدة. عموما أنها تنطوي على خطوتين والتسجيل و الاندماج.

هذه الدراسة، نقرر أن العلاقة بين الاختلاف في الصور وتسجيل نوع من التقنيات التي يمكن أن تطبيق الأنسب لتدريب التصوير المقطعي والتصوير بالرنين المغناطيسي. نستخدم ماتلاب لمعرفة النموذج الأمثل لتسجيل صورة دقيقة. كذلك، طبقنا الخوارزمية تجميع للاندماج، والتي تهدف لانتزاع معلومات من بعض الصور ثم تلتحم مع غيرها من الصور لهم حيث تكون هذه المعلومات غائبة. وكانت التطبيقات القيام بها :

- استخراج الورم لرصد نمو الورم مع مرور الوقت.
- استخراج الأنسجة الطبيعية لإضافتها إلى طريقة مختلفة للحصول على صورة واحدة من الطابع التكاملي.

كلمات البحث : الأشعة المقطعية والتصوير بالرنين المغناطيسي، صورة تسجيل، صورة الاندماج، تجميع الخوارزميات، استخراج الورم، الأنسجة الطبيعية.

Acknowledgment

First of all, I thank Allah for giving me strength and ability to complete this study.

Furthermore, I would like to express my sincere gratitude to my supervisors Dr. Cherifi Dalila and Dr. Bentarzi Hamid for their fruitful help, powerful guidance, encouragement, motivation, valuable suggestions, support and advice during this achievement work.

A special thanks to all teachers whom have done their best to transmit their knowledge effectively.

I thank all my friends for sharing their experiences and knowledge.

My appreciation goes to all INELEC staff and central library staff for their guidance and helpful throughout this research.

I wish to thank everyone who made this work possible.

Finally, I am deeply grateful to my parents for their trust everlasting love, care, and indefectible support morally and materially during all my years of studying.

Dedication

To all those whom I cherish, love and share passion with

*To my beloved mother "Leila", who has been a source of
inspiration and encouragement to me throughout my life*

*To my beloved father "Amer", who supported me my whole life,
taught me what I know, and made me who I am*

To my sister Sara and my brothers Lounes and Ahmed

To all my family and my beloved grand parents

*To the memory of my grand fathers "Ahmed" and "Lounes", may god
bless their soul*

To all my friends and especially the closest one

To all those with whom I spent wonderful moments in my life

I dedicate this modest work,

List of Tables

Table II.1: Registration Problems	13
Table II.2: Landmarks Based Registration Results	40
Table II.3: Monomodal Intensity Based Registration Results	41
Table II.4: Multimodal Intensity Based Registration	43
Table IV.1: Results Of Clustering Algorithm For Tumor Image Extraction	74
Table IV.2: Statistical Efficiency Of Clustering Algorithm For Tumor Image Extraction	76

List of Figures

FigureI-1 Brain Anatomy	4
FigureI-2 Illustration of WM,GM, and CSF segmentation from MR images	5
FigureI-3 CT Image of Brain	6
FigureI-4 CT Equipment	6
Figure I-5 MRI Image of Brain	7
Figure I-6 MRI Equipment	7
Figure I-7 PET Scan of the Brain	7
Figure I-8 Image of PET Equipment	7
Figure I-9 SPECT Image of Brain.....	8
Figure I-10 SPECT Equipment	8
Figure II.1 3D CT Dataset of a Human Head and 2D CT Slices.....	15
Figure II.2: scale parameter applied on medical image.	26
Figure II.3: rotation parameter applied on medical image.....	26
Figure II.4: shear parameter applied on medical image.	27
Figure II.5: Linear Conformal Transformation applied on a) checkboard image, b) medical image	27
Figure II.6: Affine Transformation applied on a) checkboard image, b) medical image.....	28
Figure II.7: Projective Transformation applied on a) checkboard image, b) medical image.	29
Figure II.8: Polynomial Transformation applied on a) checkboard image, b) medical image	30
Figure II.9: Examples of 2D Transformations.	32
Figure II.10: Monomodal Images (MRI).....	35
Figure II.11: Multimodal Images (MRI & CT).....	36
Figure II.12: Flow chart describing the image registration procedure.....	38
Figure II.13: Landmark Based Registration applied to MRI slice.....	39
FigureIII.1: Generic Medical Image Fusion Scheme.....	47
Figure III.2 Fused images using the XOR operator	48
Figure III.3 RGB Cube pseudocolor map of CT image	49
Figure III.4 RGB Cube pseudocolor map of MRI image	49
Figure III.5 k-means clustering method applied on a set of randomly generated points	51
Figure III.6 Fused image using the K-means algorithm for different classes of tissue	51
Figure III.7 k-means algorithm applied to MRI slice	52
Figure III.8 k-means algorithm applied to MRI slice	52
Figure III.9 k-means algorithm applied to CT slice	53
Figure III.10 k-means algorithm applied to MRI slice	53
Figure III.11 k-means algorithm applied to CT slice	53
Figure III.12 Fuzzy k-means algorithm applied to CT slice	56
Figure III.13 Fuzzy k-means algorithm applied to MRI slice.	56
Figure III.14 Fuzzy k-means algorithm applied to MRI slice.	56
Figure III.15 Fuzzy k-means algorithm applied to CT slice.	56
Figure III.16 Fuzzy k-means algorithm applied to MRI slice	56
Figure III.17 Thresholding algorithm applied to CT slice	59
Figure III.18 Thresholding algorithm applied to MRI slice.	59
Figure III.19 Otsu's algorithm applied to CT slice.	62
Figure III.20 Otsu's algorithm applied to MRI slice	62
Figure III.21 log of the histogram, result of maximum log likelihood, and Gaussian distribution of each class.	64
Figure III.22 EM Segmentation algorithm applied to CT slice	64
Figure III.23 log of the histogram, result of maximum log likelihood, and Gaussian distribution of each class.	64
Figure III.24 EM Segmentation algorithm applied to MRI slice	64

Figure III.25 log of the histogram, result of maximum log likelihood, and Gaussian distribution of each class.	65
Figure III.26 EM Segmentation algorithm applied to MRI slice	65
Figure III.27 log of the histogram, result of maximum log likelihood, and Gaussian distribution of each class.	65
Figure III.28 EM Segmentation algorithm applied to CT slice	65
Figure III.29 log of the histogram, result of maximum log likelihood, and Gaussian distribution of each class.	66
Figure III.30 EM Segmentation algorithm applied to MRI slice	66
Figure IV.1 example of the histogram.....	70
Figure IV.2 example of image before and after enhancement	70
Figure IV.3 example of tumor image extraction using morphological operations.	72
Figure IV.4 flow chart for the system for segmentation of CT and MRI brain images.....	76
Figure IV.5 extraction of normal and abnormal tissue from CT brain images.....	77
Figure IV.6 extraction of normal and abnormal tissue from MRI brain images	77
Figure IV.7 extracting tumorr from MRI image and overlay it on MRI image	79
Figure IV.8 extracting tumorr from CT image and overlay it on CT image	79
Figure IV.9 superposition of bone structure extracted from registered CT on MRI slice.	80

Abstract	I
Acknowledgements.....	IV
Dedication	V
List of tables	VI
List of figures.....	VII
Table of content.....	IX
Introduction.....	1
Chapter I: Brain Medical Imaging.....	3
I.1. Introduction	4
I.2. Brain Anatomy.....	4
I.3. Types Of Medical Imaging	5
I.3.1. Computed Tomography	6
I.3.2. Magnetic Resonance Imaging	6
I.3.3. Positron Emission Tomography	7
I.3.4. Single photon emission computed tomography	8
I.4. Conclusion.....	8
Chapter II: Medical Image Registration.....	9
II.1. Introduction	10
II.2. Role of medical image registration.....	11
II.3. Image registration problematic	12
II.4. Classification of Registration Methods	14
II.4.1. Dimensionality	15
II.4.2. Nature of registration basis (Similarity measures)	15
II.4.2.1 Landmark based registration methods	16
a. Target Registration Error	17
b. Fiducial Registration Error	18
II.4.2.2 Segmentation based registration methods.....	20

Table of Content

II.4.2.3 Voxel property based registration methods	21
a. Correlation-Coefficient	22
b. Minimizing Intensity Difference	22
c. Mutual Information	23
II.4.3. Nature of Transformation	24
II.4.3.1. Types of spatial transformations.....	25
a. Translation	25
b. Scaling	22
c. Rotation	26
d. Shear	26
II.4.3.2. Transformation Models.....	27
a. Linear conformal transformation (Rigide Transformation).....	27
b. Affine transformation	28
c. Projective transformation	29
d. Polynomial transformation	30
II.4.4. Domain of the Transformation	32
II.4.5. Interaction	34
II.4.6. Optimization Procedure	34
II.4.7. Modalities Involved in the Registration	35
II.4.8. Subject and Object	36
II.5. Image Registration methodology	37
II.6. Results and discussion	38
II.6.1. Landmark-based Image Registration	39
II.6.2. CT/CT and MRI/MRI (Monomodal) Registration using CC Optimization	40
II.6.3. CT/MRI (Multimodal) Registration using MI optimization	43
II.7. Conclusion	44
Chapter III: Medical Image Fusion	45
III.1 Introduction	46
III.2 Medical Image Fusion	46

Table of Content

III.2.1 Fusion Using Logical Operators	47
III.2.2 Fusion Using a Pseudocolor Map	48
III.2.3 Clustering Algorithms for Unsupervised Fusion of Registered Images	49
III.2.3.1.The Kmeans Algorithm	50
III.2.3.2 The Fuzzy Kmeans Algorithm	53
III.2.3.4 Threshold algorithm	57
a. Global threshold	57
b. Local Threshold	59
c. Otsu's algorithm.....	60
III.2.3.4 Brain classification based on EM segmentation.....	62
III.3. Conclusion	66
 Chapter IV: Medical Image Registration And Fusion Methods	
Implementation	67
IV .1 Introduction	68
IV.2 Brain Tumor's Extraction	69
IV.2.1 Preprocessing	69
IV.2.2 Postprocessing	70
IV.2.3 Statistics	72
IV.3 Comparative Study of Clustering Algorithms	73
IV.4 Proposed Segmentation Method.....	76
IV.5 Fusion by registration and segmentation	78
IV.5.1. Monomodal application.....	78
IV.5.2. Multimodal application	79
IV.6 Conclusion.....	80
General Conclusion And Further Work	81
Conclusion	81
Further Work.....	83
References.....	84

INTRODUCTION

Image fusion is the process of combining relevant information from two or more images into a single image. The resulting image will be more informative than any of the input images. The fusion of medical images is the process of combining two or more images acquired from same or different imaging modalities into a single image retaining important features from each.

The work is divided in two main sections: medical image registration and medical image fusion.

Image registration is a crucial step in all image analysis tasks in which the final information is gained from the combination of various data sources like in image fusion. Typically, registration is required in medicine by combining computer tomography (CT) and magnetic resonance imaging (MRI) data to obtain more complete information about the patient, monitoring tumor growth, treatment verification, comparison of the patient's data with anatomical atlases [1].

After registration, a fusion step is required for the integrated display of the data involved. An example of the use of registering different modalities can be found in radiotherapy treatment planning, where currently (CT) is used almost exclusively. However, the use of combined (MRI) and (CT) would be beneficial, as the former is adequate for delineation of tumor tissue (which has better soft tissue contrast), while the latter is needed for accurate computation of the radiation dose. Another eminent example is in the area of neurosurgery. Patients may undergo various (MRI), (CT), and (DSA) studies for anatomical reference such as ictal and interictal (SPECT) studies. Registration of the images from practically any combination will benefit the surgeon [2].

The need to register and fuse two images has arisen due to overcome many practical problems in different fields. Registration and fusion are often necessary for [3, 4]:

- Combining information from multiple imaging modalities, for example, when relating functional information from nuclear medicine images to anatomy delineated in high-resolution MR images.
- Monitoring changes in size, shape, or image intensity over time intervals that might range from a few seconds in dynamic perfusion studies to several months or even years in the study of neuronal loss in dementia.

- Relating preoperative images and surgical plans to the physical reality of the patient in the operating room during image-guided surgery or in the treatment suite during radiotherapy.
- Relating an individual's anatomy to a standardized atlas.

The project purpose is to establish the relationship between the variation in the images and the registration and fusion techniques which are appropriate to be applied in medical field.

The first chapter presents the definitions of the different types of the medical imaging techniques that can be registered. In the second chapter, a review of classification of medical image registration methods is discussed. The third chapter deals with the concept of medical image fusion process, as well as the most representative techniques reported to include several methods to combine diagnostic information. The last chapter consists of the result and discussion of image registration and fusion applications in medical field.



Brain Medical Imaging

In this chapter, the brain anatomy with the major medical imaging modalities used in brain diagnostic imaging are described. These modalities generate an image of the body either through the detection of photons or the use of electromagnetic waves.

I.1. Introduction

The field of medical imaging and image analysis has evolved as a result of the collective contributions from many areas of medicine, engineering, mathematics, and basic sciences. The overall objective of medical imaging is to acquire useful information about the organs of the body as well as the ongoing physiological and pathological processes by using external or internal sources of energy [5]. Radiology is the use of radiation for obtaining different types of imaging. Bio-Medical imaging is simply an image of a part of the human body, using radiant energy. It includes computed tomography (CT scan), positron emission tomography (PET), single photon emission computed tomography (SPECT), and magnetic resonance imaging (MRI) [6].

I.2 Brain anatomy

Since early stages of human history, the brain has been one of the most studied parts of the human anatomy. In order to provide more insight about this organ, the number of studies of the brain has been increasing during the last century. Recent techniques have allowed increasing the knowledge about the brain structures and its functioning [7].

The normal adult human brain typically weighs between 1 and 1.5 kg and has an average volume of 1,600 cm³ [18]. The basic anatomical brain structure can be seen in Fig. I.1. This organ is made of three main parts: the forebrain, midbrain, and hindbrain [7]. The Cerebellum, that is visible at the back of the brain as shown in Figure I.1(a) [19], together with the Pons and the medulla, compose the hindbrain. A detailed description of the brain anatomy is shown in Figure I.1(b) [20].

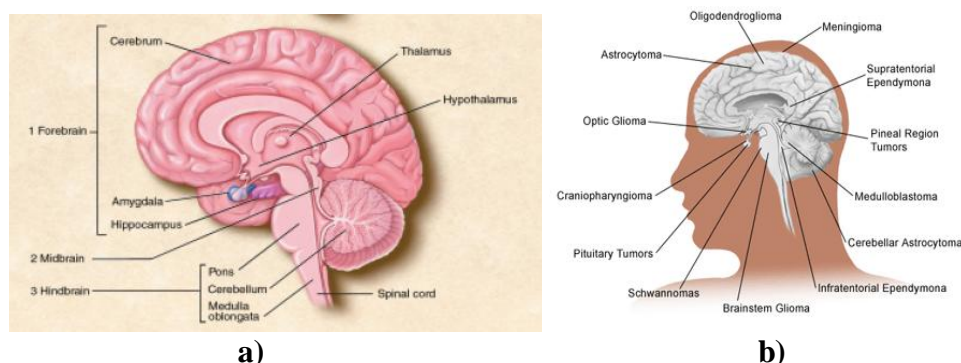


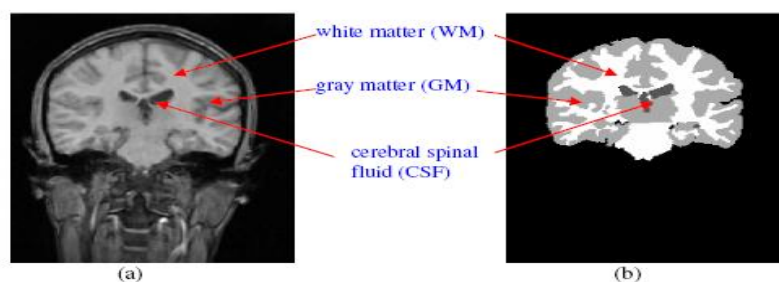
Figure I.1. Brain anatomy **a)** with all the forebrain lobes explicitly shown, along with the cerebellum and the brain stem, **b)** Detailed description parts for the five components of it.

The medulla, Pons and midbrain (tectum, tegmentum and substantia nigra) are often referred collectively as the brain stem (Figure I.1.a). These structures are almost completely enveloped by the cerebellum and telencephalon, with only the medulla visible as it merges

with the spinal cord. As for the forebrain, it is composed by the cerebrum, thalamus, and hypothalamus [7]. The cerebrum is the largest part of the human brain and is divided into four sections called “lobes” (Figure I.1.a): the frontal, parietal, occipital, and temporal lobes. In the next subsection, a more thorough review of the cerebrum is shown, as this work is mainly focused in tissue detection in that particular area of the brain.

The cerebrum is composed of an outer layer of gray matter (GM), internally supported by deep brain white matter (WM). It is responsible for the so called “higher functions”, such as conscious thinking [8]. Gray matter consists of cell bodies of the neurons, while white matter consists mostly of axons that connect neurons. These are often surrounded by a fatty insulating sheath called myelin, giving the white matter its distinctive coloration. The task of the myelin is to insulate nerve endings and enable brain signals to move smoothly [7].

The subarachnoid space, which separates the soft tissues of the brain and spinal cord from the hard surrounding bones (skull and vertebrae), is filled with cerebrospinal fluid (CSF). The choroid plexus in the ventricles produces this fluid, filling the ventricular space [9] (Figure I.1.b). The CSF is very similar to blood plasma and is the main supplier of nutrients to the brain. Figure I.2 illustrates a segmented WM, GM and CSF of brain image .



FigI.2. Illustrations of WM, GM, and CSF segmentation from MR brain images.
a) The original brain image; **b)** the segmented WM, GM and CSF of original image.

I.3 Types of Medical Imaging

Imaging has become an integral part of medical care. The ability to obtain information about the anatomic and physiologic status of the brain without the need for direct visualization has dramatically altered the practice of medicine.

Several imaging modalities have been developed and used extensively to study and to identify different types of diseases. The most common imaging techniques that are in use at present are [5]:

I.3.1 Computed Tomography

Computed Tomography (CT) scan also called computed axial tomography (CAT) scan is a series of detailed pictures of areas inside the body taken from different angles. The pictures are created by a computer linked to an x-ray machine. It is a specialized X-ray imaging technique [10, 11]. It may be performed plain or after the injection of a Contrast Agent. CT creates the image by using an array of individual small X-Ray sensors and a computer. By spinning the X-Ray source and the sensor/detectors around the patient, data is collected from multiple angles. A computer then processes this information to create an image on the video screen. These images are called sections or cuts because they appear to resemble cross-sections of the body. This technique eliminates the problem of conventional X-rays, where all the shadows overlap [12].



FigureI.3 CT Image of Brain



FigureI.4 CT Equipment

I.3.2 Magnetic Resonance Imaging

A magnetic resonance imaging (MRI) scan is a radiology technique that uses magnetism, radio waves, and a computer to produce images of body structures. The image and resolution produced by MRI is quite detailed and can detect tiny changes of structures within the body. For some procedures, contrast agents such as gadolinium are used to increase the accuracy of the images. The MRI scan can be used as an extremely accurate method of disease detection throughout the body. In the head, trauma to the brain can be seen as bleeding or swelling. Other abnormalities can be detected such as brain aneurysms, stroke, tumors of the brain, as well as tumors or inflammation of the spine. Neurosurgeons use an MRI scan not only in defining brain anatomy but in evaluating the integrity of the spinal cord after trauma. It is also used when considering problems associated with the vertebrae or intervertebral discs of the spine. MRI scan can evaluate the structure of the heart and aorta, where it can detect aneurysms or tears. It provides valuable information on glands and organs within the abdomen, and accurate information about the structure of the joints, soft tissues, and bones of the body. Often, surgery can be deferred or more accurately directed after knowing the results of MRI scan [13]. MRI scan has the advantage of avoiding x-ray radiation exposure. The benefit of the MRI scan is its

accuracy in detecting structural abnormalities of the body. Patients who have any metallic materials within the body must notify their physician prior to the examination or inform the MRI staff. Metallic chips, materials, surgical clips, or foreign material (artificial joints, metallic bone plates, or prosthetic devices, etc.) can significantly distort the images obtained by the MRI scanner. Patients who have heart pacemakers, metal implants, or metal chips or clips in or around the eyeballs cannot be scanned with the MRI because of the risk that the magnet may move the metal in these areas [14].

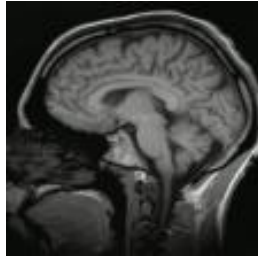


Figure I-5 MRI Image of Brain



Figure I-6 MRI Equip

I.3.3 Positron Emission Tomography

Positron emission tomography, (PET) imaging also called a (PET) scan, is a diagnostic examination that involves the acquisition of physiologic images based on the detection of radiation from the emission of positrons. Positrons are tiny particles emitted from a radioactive substance administered to the patient. PET is one of the newest and most advanced method for studying organs in the body such as the brain. Like an X-ray, or MRI scan, PET is relatively non-invasive (i.e., no surgery or opening of the body is required). Unlike X-rays and traditional MRI, PET does not produce a picture of the structure or anatomy of the brain, but rather it gives an image of brain function or physiology. In other words, it can be used to image what the brain is doing. It represents a new step forward in the way scientists and doctors look at the brain and how it functions. It measures vital functions such as blood flow, oxygen use and blood sugar (glucose) metabolism. PET scans of the heart can be used to determine blood flow to the heart. PET scans of the brain are used to evaluate patients who have memory disorders of an undetermined cause, suspected or proven brain tumors or seizure disorders. This can help doctors distinguish abnormal from normal functioning organs and tissues [15].

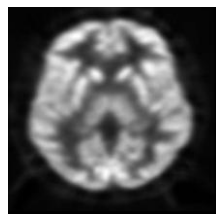


Figure I-7 PET Scan of the Brain



Figure I-8 Image of PET Equipment

I.3.4 Single photon emission computed tomography

Similar to X-ray, Computed Tomography (CT) or Magnetic Resonance Imaging (MRI), Single Photon Emission Computed Tomography (SPECT) allows us to visualize functional information about a patient's specific organ or body system [16]. As its name suggests (single photon emission), gamma ray emissions are used as the source of information, rather than X-ray transmissions used in conventional Computed Tomography. SPECT can be used to complement any gamma imaging study, and produces a true 3D representation that may be helpful in tumor imaging, infection (leukocyte) imaging, thyroid imaging or bone imaging. Because SPECT permits accurate localization in 3D space, it can be used to provide information about localized function in internal organs. Gated acquisitions are possible with SPECT, just as with planar imaging techniques. SPECT imaging is performed by using a gamma camera to acquire 3-dimensional images. The Gamma camera collects gamma rays that are emitted from the patient, aids us to reconstruct a picture of where the gamma rays originated. From this, we can determine how a particular organ or system is functioning. A computer can then be used to apply a tomographic reconstruction algorithm to the multiple projections, yielding a 3D dataset. Because SPECT acquisition is very similar to planar gamma camera imaging, the same radiopharmaceuticals may be used. If a patient attends for a nuclear medicine scan, but the images are non-diagnostic, it may be possible to proceed straight to SPECT by simply reconfiguring the camera while the patient remains on the table [17].

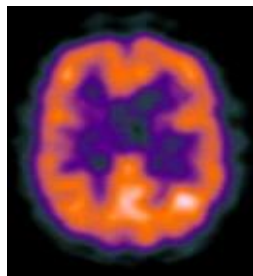


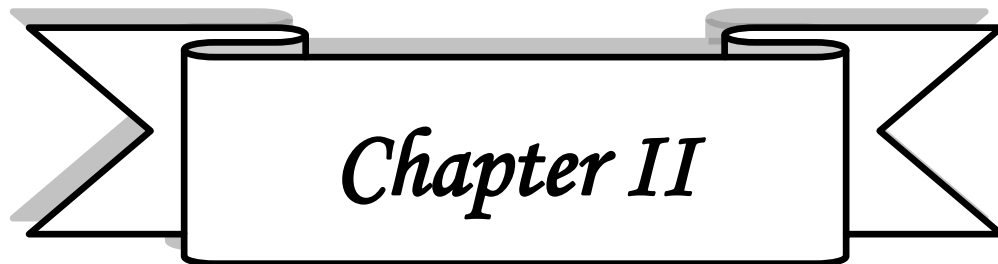
Figure I-9 SPECT Image of Brain



Figure I-10 SPECT Equipment

I.4. Conclusion

In this chapter brain anatomy and four different types of brain medical imaging are defined. These medical imaging are: Computed Tomography (CT), Magnetic Resonance Imaging (MRI), Positron Emission Tomography (PET) and Single photon emission computed tomography (SPECT).



Medical Image Registration

This chapter is dedicated for Medical image registration which has many different applications, like: monitoring changes over time in size, shape or image intensity, combining information from multiple imaging modalities (e.g. CT and MRI), and relating individual anatomies to standardized atlases. Image registration methodology and the flowchart of registration used in our work will be discussed.

II.1. Introduction

Image registration is the process of overlaying two or more images of the same scene taken at different times, from different viewpoints, and/or by different sensors. It geometrically aligns two images the reference and sensed images [1, 21, 2, 22, 23, 24, 25].

The objective of registration process is to obtain a spatial transformation of a floating image to a reference image by which a similarity measure is optimised between the two images.

By registering two images, the fusion of multimodality information becomes possible, the depth map of the scene can be determined, changes in the scene can be detected, and objects can be recognized.

Image registration can be defined as a mapping between two images both spatially and with respect to intensity. If we define these images as two 2-dimensional arrays of a given size denoted by I_1 and I_2 where $I_1(x, y)$ and $I_2(x, y)$ each map to their respective intensity values, then the mapping between images can be expressed as:

$$I_2(x, y) = g\left(I_1(f(x, y))\right) \quad (\text{II. 1})$$

where f is a 2D spatial coordinate transformation, i.e.,

$$(x', y') = f(x, y) \quad (\text{II. 2})$$

and g is 1D intensity or radiometric transformation.

The registration problem is the task involved in finding the optimal spatial and intensity transformations so that the images are matched with regard to the misregistration source. After all, if the images are matched exactly, then what information can be extracted? Finding the spatial or geometric transformation is generally the key to any registration problem. It is frequently expressed parametrically as two single-valued functions, f_x, f_y :

$$I_2(x, y) = I_1\left(f_x(x, y), f_y(x, y)\right) \quad (\text{II. 3})$$

which may be more naturally implemented. If the geometric transformation can be expressed as a pair of separable functions, i.e., such that two consecutive 1-D (scanline) operations can be used to compute the transformation,

$$f(x, y) = f_1(x)of_2(y) \quad (\text{II. 4})$$

then significant savings in efficiency and memory usage can be realized during the implementation. Generally, f_2 is applied to each row, then f_1 is applied to each column. In

classical separability the two operations are multiplied but for practical purposes any compositing operation can offer considerable high speed [3].

Image registration consists of finding the geometric (coordinate) transformation that relates two different images, source and target. Hence, when the transformation is applied to the source image, an image with the same geometry as the target one is obtained. Both images may be obtained with the same acquisition modality and illumination conditions, the transformed source image would ideally become identical to the target one. Image registration is a crucial element of computerized medical-image analysis that is also present in other nonmedical applications of image processing and computer vision [26].

II.2.Role of medical image registration

Image registration is a crucial step in all image analysis tasks in which the final information is obtained from the combination of various data from different sources, as in image fusion, change detection, and multichannel image restoration. Typically, registration is required in remote sensing (multispectral classification, environmental monitoring, change detection, image mosaicing, weather forecasting, creating super-resolution images, integrating information into geographic information systems (GIS)), in medicine (combining (CT) and MRI data to obtain more complete information about the patient, monitoring tumor growth, treatment verification, comparison of the patient's data with anatomical atlases), in cartography (map updating), and in computer vision (target localization, automatic quality control), to name a few [1].

Within the current clinical setting, medical imaging is a vital component of a large number of applications. Such applications occur throughout the clinical track of events; not only within clinical diagnosis settings, but prominently so in the area of planning, and evaluation of surgical and radiotherapeutical procedures.

Since information obtained from two images acquired in the clinical track of events is usually of a complementary nature. So, proper integration of useful data obtained from the separate images is often desired. A first step in this integration process is to bring the modalities involved into spatial alignment, produced by registration.

After registration, a fusion step is required for the integrated display of the data involved.

The use of registration of different modalities can be found in radiotherapy treatment planning, where currently CT is used almost exclusively. Where, the use of MRI and CT combined would be beneficial, as the former is better suited for delineation of tumor tissue (and has in general better soft tissue contrast), while the latter is needed for accurate

computation of the radiation dose. Another example is in the area of neurosurgery, patients may undergo various MR, CT, and DSA studies for anatomical reference; ictal and interictal SPECT studies; MEG and extra and/or intra-cranial (subdural or depth) EEG, as well as 18FDG and/or 11C-Flumazenil PET studies. Registration of the images from practically any combination will benefit the surgeon [2].

The need to register two images has arisen in many practical problems in diverse fields. Registration is often necessary for [3]:

- ✓ Integrating information taken from different sensors.
- ✓ Finding changes in images taken at different times or under different conditions.
- ✓ Inferring three dimensional information from images in which either the camera or the objects in the scene have moved.
- ✓ And for model-based object recognition

II.3. Image registration problems

To register two images, a transformation must be found so that each point in one image can be mapped to a point in the second. This mapping must optimally align the two images where optimality depends on what needs to be matched. As an example, consider two images taken of a patient using different sensors. CT scan can clearly show the structures of the patient, i.e., the bones and gross anatomy. Another scan using a sensor which is sensitive to radionucleic activity such as PET or SPECT can show metabolic activity but it can only indirectly sense a limited number of organs of normal structures. Since the two images which have different resolutions, may be taken at different times and from different viewpoints, it is not possible to simply overlay the two images. However, successful registration is capable of identifying the structural sites of metabolic activities (such as tumors) that might otherwise be difficult to ascertain [27]. In this case, registration involves finding a transformation which matches the structures found by both sensors [3].

Table II.1 gives examples of registration for each of the four classes of problems taken from computer vision and pattern recognition, medical image analysis and remotely sensed data. In this table, each class of problems is further described by its typical applications and the characteristics of methods commonly used for that class. Registration problems are by no means limited by this categorization scheme. Many problems which are combinations of these four classes of problems; arise due to images frequently taken from different perspectives and under different conditions. Furthermore, the typical applications mentioned for each class of problems are often applications in other classes as

well. Similarly, method characteristics are listed only to give an idea of the some of the more common attributes used by researchers for solving these kinds of problems. In general, methods are developed to match images for a wide range of possible distortions and it is not obvious exactly for which types of problems they are best suited. One of the objectives of this table is to present to the reader the wide range of registration problems. Not surprisingly, this diversity in problems and their applications has been the cause for the development of enumerable independent registration methodologies [3].

Table II.1: Registration Problems

Examples	Class of problems	Typical application	Characteristics of methods	Registration types
Integrate structural information from CT or MRI with functional information from radionuclenic scanners such as PET or SPECT for anatomically locating metabolic function.	Registration of images of the same scene acquired from different sensors.	Integration of information for improved segmentation and pixel classification.	Often use sensor models, need to preregister intensities, image acquisition using subject frames and fiducial markers can simplify problem.	Multimodal Registration.
	Find a match for a reference pattern in an image.	Recognizing or locating a pattern such as an atlas, map, or object model in an image.	Model-based approaches, preselected features, known properties of object, higher level matching.	Template Registration.
	Registration of images taken from different viewpoints.	Depth or shape reconstruction.	Need local transformation to account for perspective distortions, often use assumptions about viewing geometry and surface properties to reduce search, typical approach is feature correspondence but problem of occlusion must be addressed.	Viewpoint Registration.
Digital Subtraction Angiography (DSA) - registration of images before and after radio isotope injections to characterize functionality, Digital Subtraction Mammography to detect tumors, Early Cataract Detection.	Registration of images of same scene taken at different times or under different conditions.	Detection and monitoring of changes or growths.	Need to address problem of dissimilar images, i.e. registration must tolerate distortions due to change, best if can model sensor noise and viewpoint changes, frequently use Fourier methods to minimize sensitivity to dissimilarity.	Temporal Registration.

II.4. Classification of Registration Methods

There are a number of different ways and methods to classify image registration. Here, the classification of registration methods used in this work is based on the below basic criteria, each of which is again subdivided on one or two levels [30, 2]. The primary subdivisions are:

1. Dimensionality
2. Nature of registration basis
 - a. Extrinsic
 - b. Intrinsic
 - c. Non-image based
3. Nature of transformation
 - a. Rigid
 - b. Affine
 - c. Projective
 - d. Curved
4. Domain of transformation
5. Interaction
6. Optimization procedure
7. Modalities involved
 - a. Monomodal
 - b. Multimodal
 - c. Modality to model
 - d. Patient to modality
8. Subject
 - a. Intrasubject
 - b. Intersubject
 - c. Atlas
9. Object

II.4.1. Dimensionality

Dimensionality can be investigated by only spatial dimensions or spatial dimensions with time.

The further sub-division is depending on the number of spatial dimensions involved:

- 2D/2D: applied to single slices from tomographic data or any 2D image (less complex, easier and faster than 3D/3D).
- 2D/3D: may be required when establishing correspondences between 3D volumes and projections, primarily used in intra-operative procedures e.g. pre-operative 3D CT image to an intra-operative X-ray image. An example is shown in figure II.1.
- 3D/3D: applies to the registration of two tomographic datasets or one tomographic dataset and any spatial image. 3D to 3D registration is the most well developed and widely used.
- Time series of images are acquired for various reasons, such as monitoring of bone growth in children (long time interval), monitoring of tumor growth (medium interval), post-operative monitoring of healing (short interval), or observing the passing of an injected bolus through a vessel tree (ultra-short interval). If two images needed for comparing, registration will be necessary except in some instances of ultra-short time series, where the patient does not leave the scanner between the acquisition of two images.

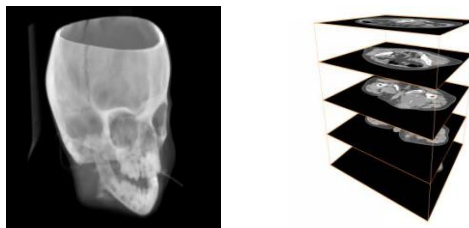


Figure II.1 3D CT Dataset of a Human Head and 2D CT Slices.

II.4.2. Nature of registration basis (Similarity measures)

The method used to measure the similarity between images is a very central part in the image registration process. The similarity measure, also referred to as the cost function, sets a limit on the best possible registration that can be achieved. The most desired feature of the cost function is that the optimum value should correspond to the transformation configuration producing a perfect match between the images. Furthermore, it should preferably be smooth and consists of few local optima, apart from the global optimum. There is a number of different families of cost functions available, which uses completely different types of features to measure the similarity.

Image based registration can be divided into extrinsic, that is based on foreign objects introduced into the imaged space, and intrinsic methods that is based on the image information as generated by the patient.

Extrinsic methods rely on artificial objects attached to the patient, objects which are designed to be well visible and accurately detectable in all of the pertinent modalities. As such, the registration of the acquired images is comparatively easy, fast, can usually be automated, and, since the registration parameters can often be computed explicitly, has no need for complex optimization algorithms

Since extrinsic methods by definition cannot include patient related image information, the nature of the registration transformation is often restricted to be rigid (translations and rotations only). Because of the rigid transformation constraint, and various practical considerations, use of extrinsic 3D/3D methods is largely limited to brain and orthopedic imaging, although markers can often be used in projective (2D) imaging of anybody area.

Intrinsic methods rely on patient generated image content only. Registration can be based on a limited set of identified salient points (landmarks), on the alignment of segmented binary structures (segmentation based), most commonly object surfaces, or directly onto measures computed from the image grey values (voxel property based) [31].

II.4.2.1 Landmark based registration methods

One of the most intuitively obvious registration procedures is based on identification of corresponding point landmarks or “fiducial markers” in the two images. For these methods, the actual similarity criterion minimises the distance between the corresponding points in I_t and I_r , respectively. This family of methods is most often referred to as landmark-based or point-based methods.

For a rigid structure, identification and location of three landmarks will be sufficient to establish the transformation between two 3D image volumes, provided the fiducial points are not all in a straight line. In practice it is usual to use more than three. The larger the number of points used, the more any errors in marking the points are averaged out. The algorithm for calculating the transformation is well known and straightforward. It involves first computing the average or centroid of each set of points. The difference between the centroids in 3D tells us the translation that must be applied to one set of points. This point set is then rotated about its new centroid until the sum of the squared distances between each corresponding point pair is minimized. The square root of

the mean of this squared distance is often recorded by the registration algorithm. It is also referred to as the root mean square (RMS) error, residual error or fiducial registration error (FRE).

A more meaningful measure of registration error is the accuracy with which a point of interest (such as a surgical target) in the two images can be aligned. This error is normally position-dependent in the image, and is called the target registration error (TRE). In practical terms, TRE, and how it varies over the field of view, is the most important parameter determining image registration quality. Fitzpatrick [32] has derived a formula to predict TRE based on corresponding point identification. The formula computes TRE from the distribution of fiducial points and the estimate of error in identifying correspondence at each point, the fiducial localization error (FLE).

Alternatively, corresponding internal anatomical landmarks may be identified by hand on each image. These must correspond to truly point-like anatomical landmarks at the resolution of the images (such as the apical turn of the cochlea), structures in which points can be unambiguously defined (such as bifurcations of blood vessels or the center of the orbits of the eyes), or surface curvature features that are well defined in 3D. Several methods have been reported to register clinical images using corresponding anatomical landmarks that have been identified interactively by a skilled user [33, 34, 35]. Assuming all markers are identified with the same accuracy, registration error as measured by TRE can be reduced by increasing the number of fiducial markers. If the error in landmark identification or FLE is randomly distributed about the true landmark position, the TRE reduces as the square root of the number of points identified, for a given spatial distribution of points. TRE values of about 2 mm at the center rising to about 4 mm at the periphery are to be expected when registering MR and PET images of the head using 12 anatomical landmarks well distributed over the image volume. For registering MR and CT images, including the skull base, typical misregistration errors (TRE values) will be about 1 mm at the center, rising to about 2 mm at the periphery for 12 to 16 landmarks [32]. Finding these landmarks automatically and reliably is difficult and remains a research issue [4].

a) Target Registration Error

A common geometrical measure, which we will call target registration error (TRE), is the displacement between two corresponding points after registration, i.e., after one of the points has been subjected to the registering transformation. The word target in the name of this error measure is meant to suggest that the error is being measured at an anatomical

position that is the target of some intervention or diagnosis. Such errors would be expected to be more meaningful than errors measured at points with no intrinsic clinical significance. We let \mathbf{p} represent a point in the first image of a pair to be registered, and \mathbf{q} a point in the second image. A registration method applied to this pair leads to a transformation \mathbf{T} that, without loss of generality, registers the first image to the second. The difference between the two vectors representing the transformed point and the corresponding point gives the target registration error. Thus,

$$\text{TRE} = \mathbf{T}(\mathbf{p}) - \mathbf{q} \quad (\text{II.5})$$

If the direction of the error is important, the vector quantity must be reported; normally, however, only the magnitude TRE of the error is reported.

b) Fiducial Registration Error

An example of an error measure that lacks the intrinsic clinical meaning associated with TRE is fiducial registration error (FRE). This error is sometimes reported for systems that achieve registration by aligning pairs of points associated with specially selected “fiducial” features that are visible in both spaces. Fiducial features are selected not because of their clinical significance, but because of their locatability. They may be part of some easily visible anatomical features or they may be the centroids of specially designed fiducial markers that have been affixed to the anatomy before imaging. In either case the word “fiducial” is meant to suggest reliability. The reliability of anatomical points is enhanced by restricting their choice to clearly visible features; the reliability of the marker derives from its design, which typically insures that it is bright enough and large enough to render a consistent centroid in each image. The reliability of a point used in any point-based registration system is directly related to the consistency with which the identical geometrical location within the fiducial feature can be identified in each image space. An error in this localization step, which is commonly called the fiducial localization error (FLE), will propagate throughout the registration process, but if the magnitude of FLE is small, it can be expected that a transformation that aligns fiducial points will align less visible target points accurately as well. Fiducial registration error is typically reported as a mean, commonly in the root-mean-square (RMS) sense of the distance between corresponding fiducial points after a point-based registration has been effected.

Thus,

$$\text{FRE}^2 = \sum_i^N |\mathbf{T}(\mathbf{p}_i) - \mathbf{q}_i|^2 \quad (\text{II.6})$$

Where N equals the number of fiducials used in the registration process and \mathbf{p}_i and \mathbf{q}_i are positions of fiducial i in the two image spaces.

TRE is more meaningful as a measure of registration success than FRE for two reasons. First, as pointed out above, TRE can be measured at clinically relevant points, whereas FRE is by definition limited to fiducial features whose positions are clinically relevant only by coincidence. Second, FRE may overestimate or underestimate registration error. The clinical relevance of TRE makes it dominant over FRE as a general measure of meaningful error, but if FRE were itself a good estimate of TRE, then it could serve as an easily measurable surrogate. Unfortunately, it is not. The first problem is underestimation. Some components of registration error will not be reflected in FRE because the registration system uses these same fiducial point locations in its determination of the registering transformation. These hidden errors come about because the system does its best, within the limits of the set of transformations at its disposal, to align fiducial points pairs identified as corresponding, regardless of whether they do indeed correspond. For example, if the transformations being considered by the registration system are limited to rigid-body motion, then fiducial localization errors of the same magnitude and direction for every fiducial in a given image space will make no contribution to FRE.

In general, for all rigid-body registration systems, to the extent that a given set of fiducial localization errors can be duplicated by means of a rigid-body motion, the registration error will be underestimated by FRE. For nonrigid motion the situation may be worse. Any set of point pairs, however badly localized in either or both spaces, can be perfectly aligned, given a sufficiently versatile set of geometrical transformations. The FLE at each of the fiducial points will be interpolated exactly or approximately at all other points. Thus, by overfitting the fiducials in one space to their positions in the other space, the transformation may produce an FRE smaller than the true TRE. This problem is less insidious if the set of transformations is justified on physical grounds, meaning that the transformations include only those physically possible between the two spaces. For example, if two images of the same head are acquired, then for multimodality registration, where the desired accuracy is of the order of one mm, only a rigid transformation is justified (unless there is intervening surgical resection). For nonrigid anatomy or intrapatient registration, the registering transformation may not reflect the physical transformation in regions where no points are available. It is helpful to view the problem of underestimation in terms of a null space. Regardless of the set of transformations, for sufficiently small errors FRE can be expected to be an approximately linear function of the

N fiducial localization errors. The input space of FRE, as function of the FLEs, will always include a null subspace, which is the space of patterns of FLEs that can be completely compensated by one of the transformations in the set. If the localization error pattern has a component in that null space, then FRE will underestimate TRE. The second problem is overestimation.

The relationship between the expected FLE and the expected TRE depends on both the number and placement of the fiducial points. For uncorrelated FLEs, the relationship for rigid-body registration has been subject to conjecture for many years but is now well understood in the RMS sense for isotropic error patterns [36, 37].

The relationship between FRE and FLE, which is due to Sibson, [38] is surprisingly simple,

$$\text{RMS}(\text{FRE}) = \left(1 - \frac{2}{N}\right)^{\frac{1}{2}} \text{RMS}(\text{FLE}) \quad (\text{II.7})$$

Where N is again the number of fiducial points used in the registration. This equation is of great importance because it provides a means to bridge.

II.4.2.2 Segmentation based registration methods

Another common group of registration methods are used to match features from segmented objects in the images. Very often surfaces of the objects are used and therefore these methods are often referred to as surface-based methods. Typically, the surface models are deformed to fit each other in the two images and the optimum is reached when they fit perfectly. The actual similarity measure can be based on either a summation of the distance between a number of points on the surfaces or some other criterion.

Segmentation based registration methods can be rigid model based, where anatomically the same structures (mostly surfaces) are extracted from both images to be registered, and used as sole input for the alignment procedure. They can also be deformable model based, where an extracted structure (also mostly surfaces, and curves) from one image is elastically deformed to fit the second image. The rigid model based approaches are probably the most popular methods currently in clinical use. Their popularity relative to other approaches is probably for a large part due to the success of the “head-hat” method, which relies on the segmentation of the skin surface from CT, MR and PET images of the head. Since the segmentation task is fairly easy to be performed, and the computational complexity relatively low, the method is still popular. Many papers aimed at automating the segmentation steps for improving the optimization performance, or otherwise

extending the method, have been published. A drawback of segmentation based methods is that the registration accuracy is limited to the accuracy of the segmentation step. Segmentation based registration is theoretically applicable to images of many areas of the body, however in practice, the application areas have largely been limited to neuroimaging and orthopedic imaging. The methods are automated but the segmentation step, is often performed semi-automatically.

With deformable models however, the optimization criterion is different. It is always locally defined and computed, and the deformation is constrained by elastic modeling constraints (by a regularization term) imposed onto the segmented curve or surface. Deformable curves appear in literature as snakes or active contours; 3D deformable models are sometimes referred to as nets. To simplify the physical modeling, the data structure of deformable models is not commonly a point set. Instead, it is often represented using localized functions such as splines. The deformation process is always done iteratively, small deformations at a time. Deformable model approaches are based on a template model that needs to be defined in one image. After that, two types of approaches can be identified: the template is either deformed to match a segmented structure in the second image. In the latter case, the fit criterion of the template can be, e.g., to lie on an edge region in the second image. Opposed to registration based on extracted rigid models, which is mainly suited for intrasubject registration, deformable models are in theory very well suited for intersubject and atlas registration, as well as for registration of a template obtained from a patient to a mathematically defined general model of the templated anatomy. A drawback of deformable models is that they often need a good initial position in order to properly converge, which is generally realized by (rigid) pre-registration of the images involved. Another disadvantage is that the local deformation of the template can be unpredictably erratic if the target structure differs sufficiently from the template structure. A typical error is that the deformable model matches the anatomy perfectly, except in the one interesting image area where a large tumor growth has appeared. In intrasubject matching of the cortical surface, this may result in entire gyri being missed or misplaced. The solution may lie locally adapting the elasticity constraints.

II.4.2.3 Voxel property based registration method

Finally, there is a group of methods, referred to as voxel-based or intensity-based methods, which calculates the overall similarity between the images from the contributions from each corresponding voxel pair in the images. The differences between the methods

within this group, regard the actual measure used, when the similarities within the voxel pairs are calculated. A more detailed description of some of these similarity criteria are presented [39].

a. Correlation-Coefficient

The image correlation coefficient (CC) is a cost function, which is limited to registration of images from the same modality or at least very similar modalities. This is because an assumption behind the measure is that the images should be linearly correlated to give good registration results. The CC measure is calculated according to the following expression:

$$cc = \frac{\sum_{i,j} [(I_1(i,j) - \bar{I}_1)(I_2(i,j) - \bar{I}_2)]}{\sqrt{\sum_{i,j} (I_1(i,j) - \bar{I}_1)^2 \sum_{i,j} (I_2(i,j) - \bar{I}_2)^2}} \quad (\text{II. 8})$$

b. Minimizing Intensity Difference

One of the simplest voxel similarity measures is the sum of squared intensity differences (SSD) between images which is minimized during registration.

For voxel locations \mathbf{x}_A in image A , within an overlap domain $\Omega_{A,B}^T$ comprising N voxels:

$$SSD = \frac{1}{N} \sum_{\mathbf{x}_A \in \Omega_{A,B}^T} |A(\mathbf{x}_A) - B^T(\mathbf{x}_A)|^2 \quad (\text{II. 9})$$

The SSD measure is very sensitive to a small number of voxels that have very large intensity differences between images A and B . This might arise, if contrast material is injected into the patient between the acquisition of images A and B , or if the images are acquired during an intervention and instruments are in different positions relative to the subject in the two acquisitions. The effect of these “outlier” voxels can be reduced by using the sum of absolute differences, SAD rather than SSD:

$$SAD = \frac{1}{N} \sum_{\mathbf{x}_A \in \Omega_{A,B}^T} |A(\mathbf{x}_A) - B^T(\mathbf{x}_A)| \quad (\text{II. 10})$$

The correlation coefficient can be normalized by cross correlation measure C .

$$C = \frac{1}{N} \sum_{i,j} I_1(i,j) \times I_2(i,j) \quad (\text{II. 11})$$

c. Mutual Information

Mutual information (MI) and normalised mutual information (NMI) based on image intensity values have been frequently used similarity measures for medical image registration during recent years [40, 41, 42, 43]. The criteria are general in their nature and can be used for both intra- and inter-modality registration. They measure the amount of information that one image contains about another image. Furthermore, the criterion assumes that the MI of the intensity values of corresponding voxel pairs, summed over all voxels in the images, is maximal when the images are geometrically aligned. The MI can be maximised by minimising the dispersion of the joint histogram of the two images to be registered.

$$MI = p(x, y) \times \log(p(x, y)) - p(x) \times \log(p(x)) - p(y) \times \log(p(y)) \quad (\text{II. 12})$$

The NMI criterion has been shown to produce at least as good results as the MI criterion and in some cases even better results [44]. A benefit of the NMI criterion is the amount of insensitivity of overlap between the image volumes. The NMI criterion can be mathematically expressed as:

$$NMI(I_1, I_2) = \frac{\sum_{i=1}^n H_1(i) \log H_1(i) + \sum_{j=1}^n H_2(j) \log H_2(j)}{\sum_{i=1}^n \sum_{j=1}^n H_{12}(i, j) \log H_{12}(i, j)} \quad (\text{II. 13})$$

where the normalised joint histogram and marginal histograms of the images I_1 and I_2 are denoted H_{12} , H_1 , and H_2 , respectively. Finally, i and j correspond to specific histogram levels and n is the number of bins in the histograms [39].

The voxel property based registration methods stand apart from the other intrinsic methods by the fact that they operate directly on the image grey values, without prior data reduction by the user or segmentation. There are two distinct approaches: the first is to immediately reduce the image grey value content to a representative set of scalars and orientations, the second is to use the full image content throughout the registration process. Principal axes and moments based methods are the prime examples of reductive registration methods. Within these methods the image centre of gravity and its principal orientations (principal axes) are computed from the image zeroth and first order moments. Registration is then performed by aligning the centre of gravity and the principal orientations. Sometimes, higher order moments are also computed and used in the process. The result is usually not very accurate, and the method is not equipped to handle differences in scanned volume well, although some authors attempt to remedy this latter problem. Despite its drawbacks, principal axes methods are widely used in registration

problems that require no high accuracy, because of the automatic and very fast nature of its use, and the easy implementation. The method is used primarily in the re-alignment of scintigraphic cardiac studies (even intersubject), and as a coarse pre-registration in various other registration areas. Moment based methods also appear as hybridly classified registration methods that use segmented or binarized image data for input. In many applications, pre-segmentation is mandatory in order for moment based methods to produce acceptable results.

Voxel property based methods using the full image content are the most interesting methods researched currently.

Theoretically, these are the most flexible of registration methods. Unlike other methods, they do not start with reducing the grey valued image to relatively sparse extracted information, but use all of the available information throughout the registration process. Although voxel property based methods have been around a long time, their use in extensive 3D/3D clinical applications has been limited by the considerable computational costs. An increasing clinical call for accurate and retrospective registration, along with the development of ever-faster computers with large internal memories, have enabled full-image-content methods to be used in clinical practice. Although they have not yet been introduced in time-constrained applications such as intra-operative 2D/3D registration. Methods using the full image content can be applied in almost any medical application area, using any type of transformation.

II.4.3. Nature of Transformation

The usual mathematical representation of an image is a function of two spatial variables $f(x, y)$. The value of the function at a particular location (x, y) represents the intensity of the image at that point. The term transform refers to an alternative mathematical representation of an image. This section defines several important transforms and shows examples of their application to image processing.

Determining the parameters of the spatial transformation needed to bring the images into alignment is key to the image registration process.

The most fundamental characteristic of any image registration technique is the type of spatial transformation or mapping needed to properly overlay two images. Although many types of distortion may be present in each image, the registration technique must select the class of transformation which will remove only the spatial distortions between images due to differences in acquisition and not due to differences in scene characteristics that are to

be detected. The primary general transformations are affine, projective, perspective, and polynomial.

These are all well-defined mappings of one image onto another. Given the intrinsic nature of imagery of nonrigid objects, it has been suggested [27] that some problems, especially in medical diagnosis, use fuzzy or probabilistic transformations.

The different transformation classes and their properties are defined as follows:

II.4.3.1. Types of spatial transformations

Spatial transformations map pixel locations of an input image to new locations in an output image. Determining the parameters of the spatial transformation needed to bring the images into alignment is key to the image registration process.

a. Translation

Translation is a transformation of the x-y plane that moves graphically an object toward or away from the origin of the surface in the x or y direction. For example, moving an object from point A (x1, y1) to point B (x2, y2) is a translation operation in which an object is being moved (y2 – y1) points in the y-direction.

$$\text{Translation (a, b): } (x, y) \rightarrow (a + x, b + y) \quad \begin{bmatrix} x \\ y \end{bmatrix} + \begin{bmatrix} a \\ b \end{bmatrix} = \begin{bmatrix} x + a \\ x + b \end{bmatrix} \quad (\text{II. 14})$$

The translating matrix is:

$$T = \begin{bmatrix} 1 & 0 & 0 \\ 0 & 1 & 0 \\ t_x & t_y & 1 \end{bmatrix} \quad (\text{II. 15})$$

Where:

t_x specifies the displacement along the x axis

t_y specifies the displacement along the y axis.

b. Scaling

Scale resizes the image to make it bigger or smaller than the original image.

$$\text{Scale(a, b) : } (x, y) \rightarrow (ax, by) \quad \begin{bmatrix} a & 0 \\ 0 & b \end{bmatrix} \begin{bmatrix} x \\ y \end{bmatrix} = \begin{bmatrix} ax \\ by \end{bmatrix} \quad (\text{II. 16})$$

So the scaling matrix is:

$$\begin{bmatrix} s_x & 0 & 0 \\ 0 & s_y & 0 \\ 0 & 0 & 1 \end{bmatrix} \quad (\text{II. 17})$$

Where:

s_x specifies the scale factor along the x axis

s_y specifies the scale factor along the y axis.

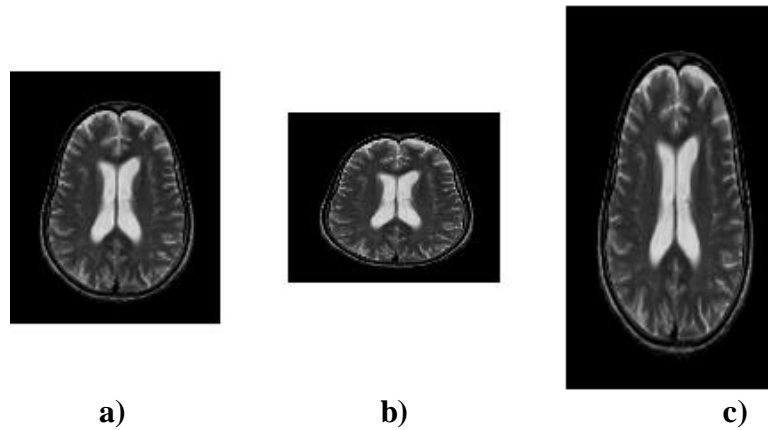


Figure II.2: Scale parameter applied to medical image. **a)**original Image, **b)**scale along x-axis, **c)** scale along y-axis

c. Rotation

Rotation moves an object by a fixed angle around the centre of the plane.

Rotate (θ): $(x, y) \rightarrow (x\cos\theta + y\sin\theta, -x\sin\theta + y\cos\theta)$

$$\begin{bmatrix} \cos\theta & \sin\theta \\ -\sin\theta & \cos\theta \end{bmatrix} \begin{bmatrix} x \\ y \end{bmatrix} = \begin{bmatrix} x\cos\theta + y\sin\theta \\ -x\sin\theta + y\cos\theta \end{bmatrix} \quad (\text{II. 18})$$

The rotation matrix is:

$$R = \begin{bmatrix} x\cos\theta & x\sin\theta & 0 \\ -x\sin\theta & y\cos\theta & 0 \\ 0 & 0 & 1 \end{bmatrix} \quad (\text{II. 19})$$

Where:

θ specifies the angle of rotation.

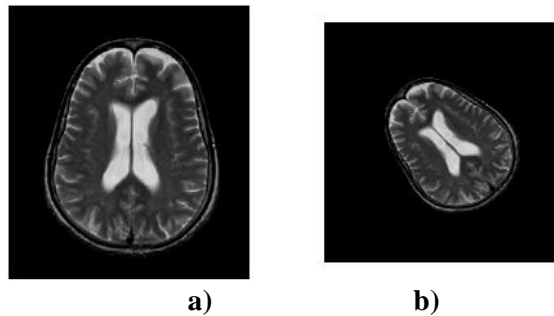


Figure II.3: rotation parameter applied to medical image. **a)**original image, **b)**rotated image

d. Shear

Shearing transformation skews objects based on a shear factor.

$$\text{Shear } (a, b): (x, y) \rightarrow (x + ay, y + bx) \quad \begin{bmatrix} 1 & a \\ b & 1 \end{bmatrix} \begin{bmatrix} x \\ y \end{bmatrix} = \begin{bmatrix} x + ay \\ y + bx \end{bmatrix} \quad (\text{II. 20})$$

The shearing matrix is:

$$\text{Sh} = \begin{bmatrix} 1 & sh_y & 0 \\ sh_x & 1 & 0 \\ 0 & 0 & 1 \end{bmatrix} \quad (\text{II. 21})$$

Where:

sh_y specifies the shear factor along the x axis

sh_x specifies the shear factor along the y axis.

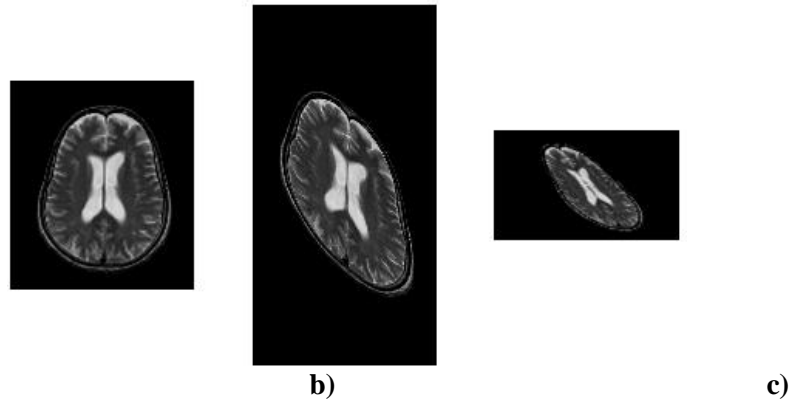


Figure II.4: Shear parameter applied to medical image. **a)** original image, **b)** shear along x-axis, **c)** shear along y-axis.

II.4.3.2. Transformation Models

Several transformation models may be employed for the global medical image registration. The most representative include the rigid, the affine, the projective and the curved or polynomial transformations.

a. Linear Conformal Transformation (Rigid Transformation)

Linear conformal transformation is composed of a combination of rotation, translation, and scale change. It accounts for object or sensor movement in which objects retain their relative shape and size (Shapes and angles are preserved). Use this transformation when shapes of the input image are unchanged, but the image is distorted by combination of translation, rotation, and scaling. Parallel lines remain parallel, straight lines remain straight.

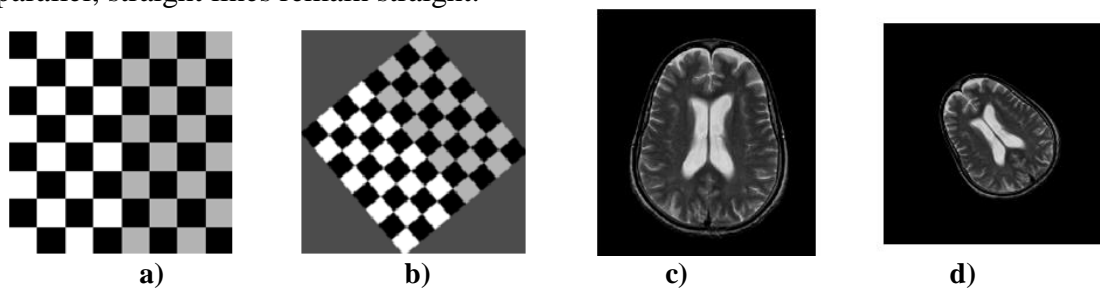


Figure II.5: Linear Conformal Transformation applied to checkerboard image and medical image. **a)** original checkerboard image, **b)** transformed checkerboard image, **c)** original medical image, **d)** transformed medical image.

The rigid transformation maintains the distance between any two points in the transformed image. The mathematical expression of the transformation for the 3-D case is given by:

$$\begin{pmatrix} x' \\ y' \\ z' \end{pmatrix} = \begin{pmatrix} 1 & 0 & 0 \\ 0 & \cos(t_x) & -\sin(t_x) \\ 0 & \sin(t_x) & \cos(t_x) \end{pmatrix} \begin{pmatrix} \cos(t_y) & 0 & \sin(t_y) \\ 0 & 1 & 0 \\ -\sin(t_y) & 0 & \cos(t_y) \end{pmatrix} \begin{pmatrix} \cos(t_z) & -\sin(t_z) & 0 \\ \sin(t_z) & \cos(t_z) & 0 \\ 0 & 0 & 1 \end{pmatrix} \begin{pmatrix} x \\ y \\ z \end{pmatrix} + \begin{pmatrix} dx \\ dy \\ dz \end{pmatrix} \quad (\text{II. 22})$$

Where t_x , t_y , , and t_z , represent the rotation angles and dx , dy , and dz represent the translation displacements along the x , y , and z axes, respectively.

For a linear conformal transformation:

$$[u \ v] = [x \ y \ 1] * T \quad \text{where } T = \begin{bmatrix} s_c & -s_s \\ s_s & s_c \\ t_x & t_y \end{bmatrix} \quad (\text{II. 23})$$

T is a 3-by-2 matrix that depends on four unknowns parameters : s_c , s_s , t_x , t_y .

At least two control-point pairs are needed to determine the four unknown coefficients.

$$s_c = \text{scale} * \cos(\text{angle}) \quad (\text{II. 24})$$

$$s_s = \text{scale} * \sin(\text{angle}) \quad (\text{II. 25})$$

b. Affine Transformation

Affine transformation is more general than linear conformal and can therefore be used for more complicated distortions. It is composed of a combination of rotation, translation, shearing and scaling. Linear conformal transformation is a subset of affine transformation. Use this transformation when shapes of the input image exhibit shearing. Parallel lines remain parallel, straight lines remain straight, but rectangles become parallelograms.

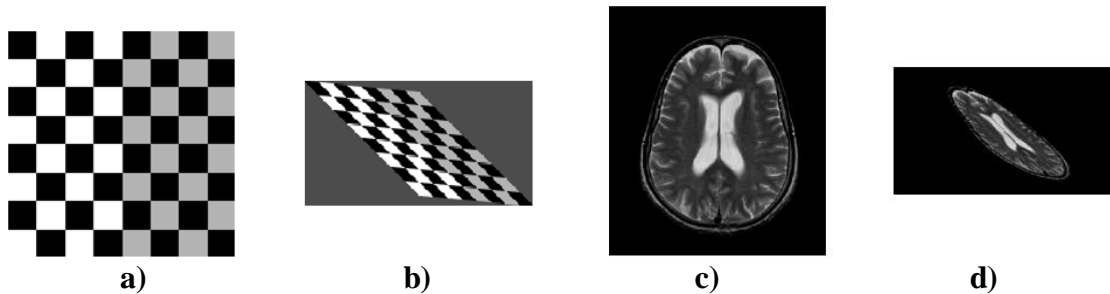


Figure II.6: Affine Transformation applied to checkerboard image and medical image. **a)** original checkerboard image, **b)** transformed checkerboard image, **c)** original medical image, **d)** transformed medical image.

The affine transformation can be decomposed into a linear transformation and a simple translation. In the 3-D case, it can be mathematically expressed as follows:

$$\begin{pmatrix} x' \\ y' \\ z' \end{pmatrix} = \begin{pmatrix} a_1 & a_2 & a_3 \\ a_1 & b_2 & b_3 \\ c_1 & c_2 & c_3 \end{pmatrix} \begin{pmatrix} x \\ y \\ z \end{pmatrix} + \begin{pmatrix} dx \\ dy \\ dz \end{pmatrix} \quad (\text{II. 26})$$

The affine transformation is completely defined by nine independent parameters (a_i, b_i, c_i) for $i= 1, 2, 3$ and $dx, dy,$ and dz , whereas, in the 2-D case, the affine transformation is defined by six independent parameters.

For an affine transformation:

$$[u \ v] = [x \ y \ 1] * T \quad \text{where } T = \begin{bmatrix} A & D \\ B & E \\ C & F \end{bmatrix} \quad (\text{II. 27})$$

T is a 3-by-2 matrix.

At least 3 control-point pairs are needed to obtain the 6 unknown coefficients.

c. Projective Transformation

Projective transformations account for distortions due to the projection of objects for varying distances to the sensor on the image plane. Use this transformation when the scene appears tilted. In a projective transformation, quadrilaterals map to quadrilaterals. The projective transformation maps any straight line in the original image onto a straight line in the transformed image. Parallelism is not preserved, parallel lines converge toward vanishing points (which may or may not fall within the image).

Affine transformations are a subset of projective transformations.

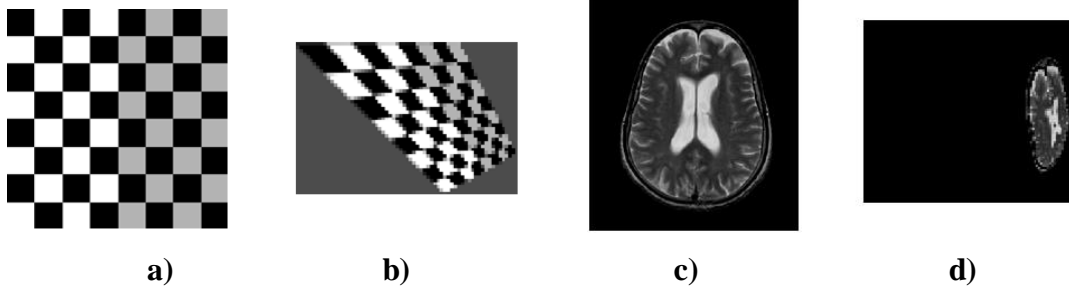


Figure II.7: Projective Transformation applied to checkerboard image and medical image. **a)** original checkerboard image, **b)** transformed checkerboard image, **c)** original medical image, **d)** transformed medical image.

The mathematical expression of the transformation for the 2-D case is given by

$$\begin{pmatrix} u \\ v \\ w \end{pmatrix} = \begin{pmatrix} a_{11} & a_{12} & a_{13} \\ a_{21} & a_{22} & a_{23} \\ a_{31} & a_{32} & a_{33} \end{pmatrix} \begin{pmatrix} x \\ y \\ 1 \end{pmatrix} \quad (\text{II. 28})$$

and,

$$\begin{pmatrix} x' \\ y' \end{pmatrix} = \begin{pmatrix} \frac{u}{w} \\ \frac{v}{w} \end{pmatrix} \quad (\text{II. 29})$$

Where w represents the extra homogeneous coordinate and u and v are dummy variables. The projective transformation is mainly employed in the 2-D case, strongly resembles the bilinear, and is completely defined by nine independent parameters (a_{11}, \dots, a_{33}).

For a projective transformation:

$$[u_p \quad v_p \quad w_p] = [x \quad y \quad w] * T \quad (\text{II.30})$$

Where,

$$T = \begin{bmatrix} A & D & G \\ B & E & H \\ C & F & I \end{bmatrix} \quad (\text{II.31})$$

with

$$u = \frac{u_p}{w_p}; \quad v = \frac{v_p}{w_p} \quad (\text{II.32})$$

T is a 3-by-3 matrix, where all nine elements are different.

At least 4 control-point pairs are needed to obtain the 9 unknown coefficients.

d. Polynomial Transformation

A polynomial transformation is one of the general transformations (in which affine is the simplest) and can account for many types of distortions so long as the distortions do not vary too much in the image. In the polynomial transformation, polynomial functions of x and y determine the mapping. This transformation may be used when objects in the image are curved. The higher the order of the polynomial, the better fitting, but the result can contain more curves than the base image.

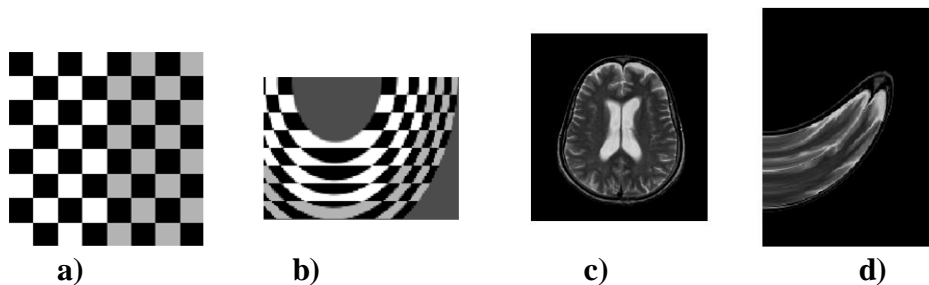


Figure II.8: Polynomial Transformation applied to checkerboard image and medical image. **a)** original checkerboard image, **b)** transformed checkerboard image, **c)** original medical image, **d)** transformed medical image.

The bilinear transformation is the simplest polynomial transformation, which maps straight lines from the original image to curves. It can be expressed for the 3-D case as:

$$\left\{ \begin{array}{l} x' = \alpha_0 + \alpha_1x + \alpha_2y + \alpha_3z + \alpha_4xy + \alpha_5yz + \alpha_6zx + \alpha_7xyz \\ y' = b_0 + b_1x + b_2y + b_3z + b_4xy + b_5yz + b_6zx + b_7xyz \\ z' = c_0 + c_1x + c_2y + c_3z + c_4xy + c_5yz + c_6zx + c_7xyz \end{array} \right\} \quad (\text{II. 33})$$

The bilinear transformation is completely defined by 24 independent parameters (a_i, b_i, c_i) for $i = 0, 1, 2, \dots, 7$. For the 2-D case, eight independent parameters completely define the bilinear transformation.

For the polynomial transformation:

$$u = X * A \quad ; \quad v = X * B \quad (\text{II. 34})$$

where,

$$A = \frac{x}{u} \quad ; \quad B = \frac{x}{v} \quad (\text{II. 35})$$

The matrix X depends on the order of the polynomial. If X is M-by-K, where

$$K = \frac{(\text{order}+1)*(\text{order}+2)}{2} \quad (\text{II. 36})$$

So, A and B will be vectors of length K.

➤ Second-Order Polynomials

For a second-order polynomial transformation,

$$[u \ v] = [1 \ x \ y \ (x * y) \ x^2 \ y^2] * T \quad (\text{II. 37})$$

Both u and v are second-order polynomial of x and y. Each second-order polynomial has six terms. To determine all coefficients, T is 6-by-2 matrix.

At least 6 control-point pairs are needed to solve for the 12 unknown coefficients.

➤ Third-Order Polynomials

For a third-order polynomial transformation:

$$[u \ v] = [1 \ x \ y \ (x * y) \ x^2 \ y^2 \ (y * x^2) \ (x * y^2) \ x^3 \ y^3] * T \quad (\text{II. 38})$$

Both u and v are third-order polynomials of x and y. Each third-order polynomial has ten terms. To determine all coefficients, T is 10-by-2 matrix.

At least 10 control-point pairs are needed to solve for the 20 unknown coefficients.

➤ Fourth-Order Polynomials

For a fourth-order polynomial transformation:

$$[u \ v] = [1 \ x \ y \ (x * y) \ x^2 \ y^2 \ (y * x^2) \ (x * y^2) \ x^3 \ y^3 \ (x^3 * y) \ (x^2 * y^2) \ (x * y^3) \ x^4 \ y^4] * T \quad (\text{II. 39})$$

Both u and v are fourth-order polynomial of x and y . Each fourth-order polynomial has fifteen terms. T gives all coefficients, which has size 15-by-2.

At least 15 control-point pairs are needed to solve for the 30 unknown coefficients.

It can be noticed that when transform type is linear conformal, affine, projective, or polynomial, and input points and base points have the minimum number of control points needed for a particular transformation, the coefficients will be found exactly. If input points and base points include more than the minimum number of points, squares solution is investigated.

II.4.4. Domain of the Transformation

It can be distinguished between global and local transformations.

In global one, the transformation is applied to the complete image. In this transformation, a single mathematical expression applies to an entire image.

In local one, the transformation is applied separately to different parts of the image, and each subsection has their own transformation. A local transformation consists at least of two transformations on sub-images that cannot be described as a global transformation. In this transformation, different mathematical expressions may be applied to different regions within an image.

Figure II.9 shows examples of all transformation types mentioned previously.

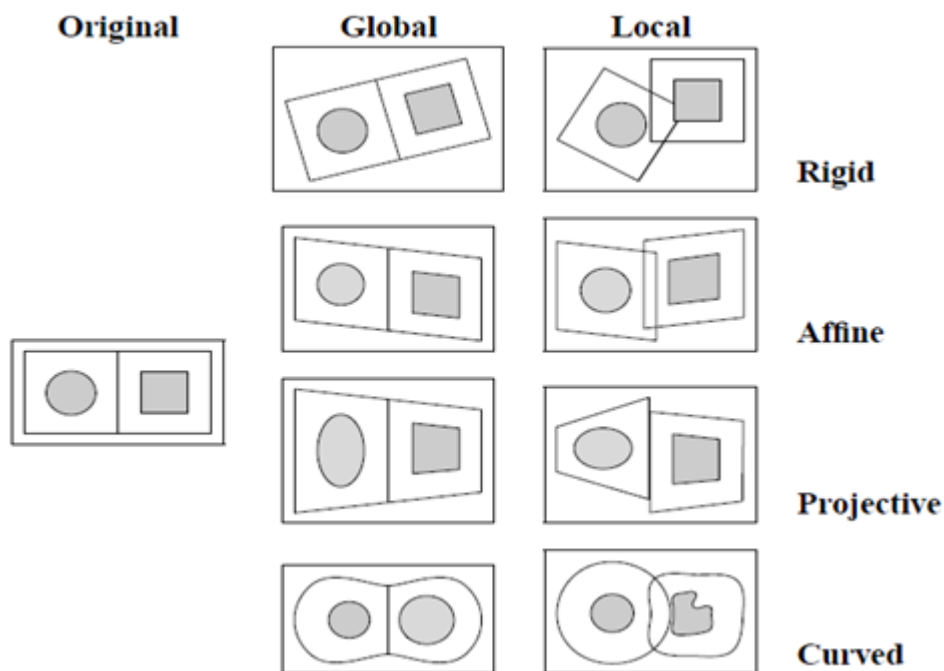


Figure II.9: Examples of 2D Transformations.

Local transformations are seldom used directly, because they may violate the local continuity and bijectiveness of the transformations, which impairs straightforward image resampling when applying the transformation to the image. The term local transformation is reserved for transformations that are composites of at least two transformations determined on sub-images that cannot be generally described as a global transformation. Hence, a single transformation computed on some volume of interest of an image, is a global transformation, except that “global” now refers to the new image, which is a sub-image of the original. This definition, perhaps confusingly, does not impair a global transformation to be computed locally, e.g., some applications compute a global rigid transformation of an image of the entire head based on computations done in the area of the facial surface only. Local rigid, affine, and projective transformations occur only rarely in the literature, although local rigid transformations may appear embedded in local curved transformations [28, 29]. Some problems that are intrinsically locally rigid (such as the registering of individual vertebrae from images of the spinal column) are in registration tasks often solved by splitting the image in images meeting the global rigid body constraint.

In recently published registration papers, as a rule, rigid and affine transformations are global, and curved transformations are local. This makes sense, given the physical model underlying the curved transformation type, and given that the rigid body constraint is –globally, or in well defined sub-images– approximately met in many common medical images. Affine transformations are typically used in instances of rigid body movement where the image scaling factors are unknown or suspected to be incorrect, (notably in MR images because of geometric distortions). The projective transformation type has no real physical basis in image registration except for 2D/3D registration, but is sometimes used as a “constrained-elastic” transformation when a fully elastic transformation behaves inadequately or has too many parameters to solve for. The projective transformation is not always used in 2D/3D applications: even though projections will always figure in the problem, the transformation itself is not necessarily projective but may be rigid, if it applies to the 3D image prior to its projection to the 2D image.

Since local information of the anatomy is essential to provide an accurate local curved transformation, applications are nearly always intrinsic, mostly deformable model based or using the full image content, and mostly semi-automatic, requiring a user-identified initialization. They appear almost solely using anatomical images (CT, MR) of

the head, and are excellently suited for intersubject and image to atlas registration. Many methods require a pre-registration (initialization) using a rigid or affine transformation.

The global rigid transformation is used most frequently in registration applications. It is popular because in many common medical images the rigid body constraint is approximately satisfied. Furthermore, it has relatively few parameters to be determined, and many registration techniques are not equipped to supply a more complex transformation. The common application area is the human head [30].

II.4.5. Interaction

Interaction within the registration process can be interactive, semi-automatic or automatic.

Interactive registration is done by the user himself, assisted by software which supplies a visual or numerical impression of the current transformation. This method is little in use in clinical applications.

In Semi-automatic registration a distinction is drawn between two different approaches which are initialization of the algorithm is done by the user (e.g. through segmentation of data) and steering by user interaction (rejecting or accepting suggested registration hypotheses).

In the automatic case, the user only inputs the image data and needed information. There is no best approach; many recent methods have a trade-off between minimal interaction and speed, accuracy, or robustness. So, some users prefer algorithms with human interaction, whereas others want no-human-interactions.

II.4.6. Optimization Procedure

The parameters that make up the registration transformation can either be computed directly, i.e., determined in an explicit fashion from the available data, or searched for, i.e., determined by finding an optimum of some function defined on the parameter space. In the former case, the manner of computation is completely determined by the paradigm. The only general remark that can be made is that the use of computation methods is restricted, completely to applications relying on very sparse information, e.g., small point sets. In the case of optimization, registration can formulate the paradigm in a standard mathematical function of the transformation parameters to be optimized. This function attempts to quantify the similarity as dictated by the paradigm between two images given a certain transformation. Such functions are generally less complex in monomodal registration applications, since the similarity is more straightforward to define. Hopefully, the

similarity function is well-behaved (quasi-convex) so one of the standard and well-documented optimization techniques can be used.

The goal of the optimisation algorithm is to find the optimal cost function value, by iteratively selecting steps in the transformation parameter space. This is done accordingly to some strategy, which is designed to finally lead to the global optimization.

Different optimisation methods are classified into two families.

First, there are the local optimisation methods, which always select the next step in the parameter space in a local surrounding of the current position. Typically, steps are not allowed to a parameter configuration corresponding to a worse cost function value than the recent one, which is considered as “greedy” methods. These algorithms are fast methods, but its drawback is the risk to get caught in local optima of the cost function. Some typical methods from this family are the simplex method [45], Powell’s method [46], and gradient descent based methods [47].

Another family of optimisation methods are the global optimisation methods, which searches the parameter space in a more global way. They allow steps to worse configurations than the best one so far, which makes the methods less sensitive to local optima of the cost function. However, these methods are usually slower than local optimisation methods. Some examples of global optimisation algorithms are methods based on the simulated annealing concept [48, 49] or genetic algorithms [50, 39].

II.4.7. Modalities Involved in the Registration

There are three main classes of registration based on the modalities: Monomodal, Multimodal and Modality to model.

In monomodal applications, both images are of the same modality e.g. only CT images or just x-Ray or ultrasound data. Growth monitoring and subtraction imaging are key domains for monomodal registration. An example is shown in figure II.10.

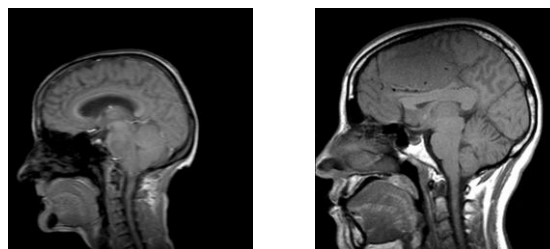


Figure II.10: Monomodal Images (MRI).

Unlike monomodal, in multimodal registration the images to be registered are of different modalities as shown in figure II.11. There are several examples of multi-modality

registration algorithms in the medical imaging field. Examples include registration of brain CT/ MRI images or whole body PET/ CT images for tumor localization. Registration of contrast-enhanced CT images against non-contrast-enhanced CT images for segmentation of specific parts of the anatomy and also registration of ultrasound and CT images for prostate localization in radiotherapy are widely used.

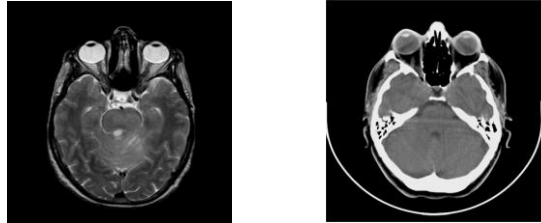


Figure II.11: Multimodal Images (MRI & CT).

Modality to model class includes only one image; the other modality is a model. An example is the registration of an MR brain image to a mathematically defined compartmental model of gross brain structures. It is used for finding anomalies relative to normalized structures.

II.4.8. Subject and Object

The subject can be differentiated between intrasubject, intersubject and Atlas. Intrasubject applications involve only images acquired from a single patient. It is the most common registration method, whereas intersubject registrations use two images of different patients (or a patient and a model) for the registration. Atlas registration is defined as one image is acquired from a single patient and the other image is somehow constructed from an image information database.

Intrasubject registration is by far the most common of the three, used in diagnostic and interventional procedure. Intersubject and atlas registration appear mostly in 3D/3D MR or CT brain image applications. There are changes in shape and size as well as great changes in topology. The nature of the registration transformation is mostly curved. These applications are always intrinsic, either segmentation based or voxel property based, using the full image content. A manual initialization is frequently desired. Some applications use rigid transforms, but their application is limited. Others use anatomical landmarks for a deformation basis of a curved transformation; unfortunately such applications often require the transformation in large image areas to be interpolated from the nearest landmark transformations, which may prove unreliable. The use of intersubject and atlas matching can notably be found in the areas of gathering statistics on the size and shape of specific

structures, finding (accordingly) anomalous structures, and transferring segmentations from one image to another.

In medical image registration, no overall procedure has been found until now. In general, the treatment is done separately on the following parts of the human body such as head, thorax, abdomen, pelvis and perineum, limbs, spine and vertebrae.

II.5. Image Registration methodology

An important part in the image fusion process is the image registration, which refers to the process of aligning or fitting different image datasets to each other. There are a number of different ways to classify image registration methods. Here, mainly three different cooperative parts related to the evaluation of the registration algorithm will be considered.

First, there is the similarity measure, which is used as the criterion to decide when the images fit best to each other. Another part is the transformations, which are applied to one of the images, referred to the target image I_t , to alter the relative alignment in relation to the reference image I_r . Finally, the optimisation algorithm is used to find the optimum value of the similarity measure by applying different sets of transformation parameters in an ordered way until the optimum will be found.

In a typical registration process, the following steps are iterated until convergence is reached according to the optimisation method. First, a transformation is applied to the target image. In the next step, the similarity measure is evaluated from the voxel values in the reference image and the transformed target image. If the method has not converged, a new set of transformation parameters is selected and the procedure is repeated. In figure II.12, a flow chart describing the image registration procedure is illustrated.

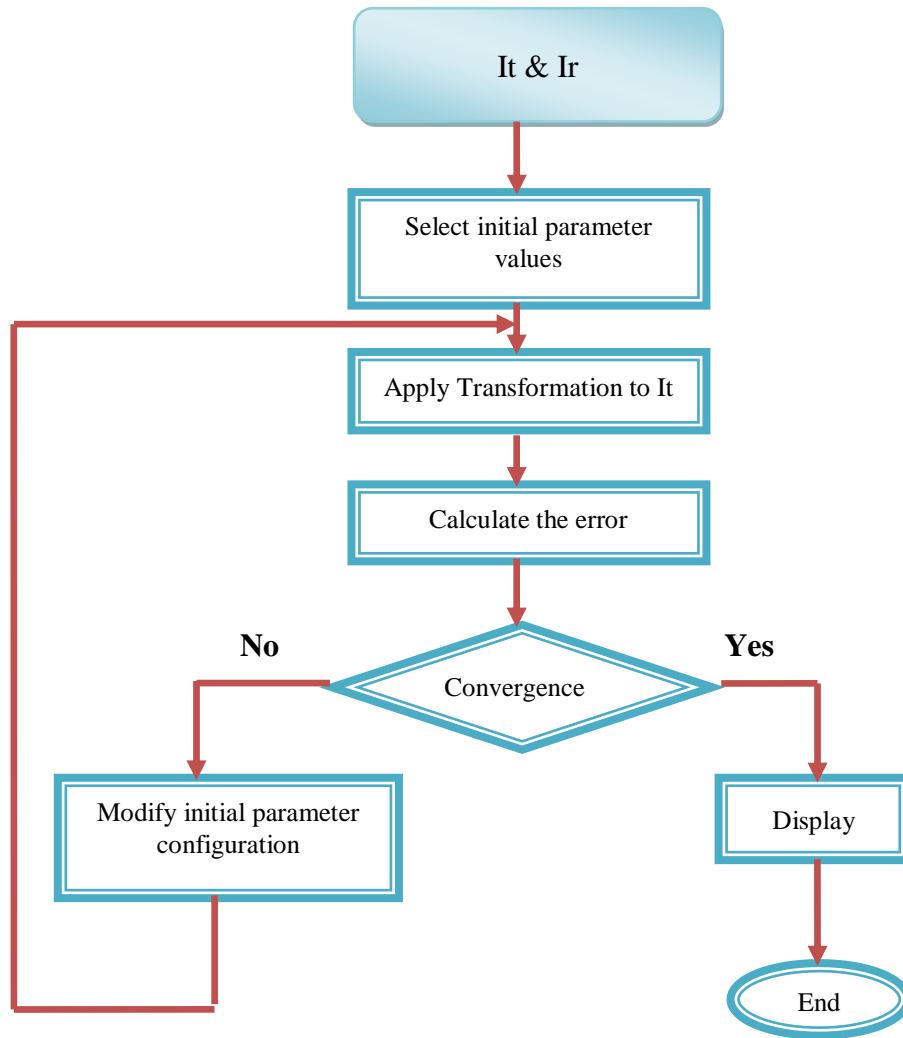


Figure II.12: Flow chart describing the image registration procedure.

II.6. Results and discussion

As stated in this chapter, medical image registration has a wide range of potential applications. These include:

- Combining information from multiple imaging modalities, for example, when relating functional information from nuclear medicine images to anatomy delineated in high-resolution MR images.
- Monitoring changes in size, shape, or image intensity over time intervals that might range from a few seconds in dynamic perfusion studies to several months or even years.
- Relating preoperative images and surgical plans to the physical reality of the patient in the operating room during image-guided surgery or in the treatment suite during radiotherapy.
- Relating an individual's anatomy to a standardized atlas.

II.6.1. Landmark-based image registration

As defined in the previous sections in this chapter, image registration can be based on predefined landmark points or fiducial markers, which are visible in images to be registered. The landmarks can be artificial or anatomical landmarks. In this section we will define and use anatomical landmarks. The aim of the first task is to plan which points could be used for registration and secondly, see how much the determination of landmarks is operator dependent.

A 2D landmark based registration algorithm of two images using rigid and affine registration is implemented. First, different numbers of landmark points have been tested at different positions. Next, landmarks have been marked to the images, then the coordinates of the landmarks and the pictures have been saved to be later used. After testing the algorithm with several landmarks defined previously, the registration parameters (translation, rotation and scale) have been saved, which the algorithm calculates. FRE and TRE are measured using equations (II.5) and (II.6). The error of the transformation parameters found is also calculated. The results are shown in figure II.13:

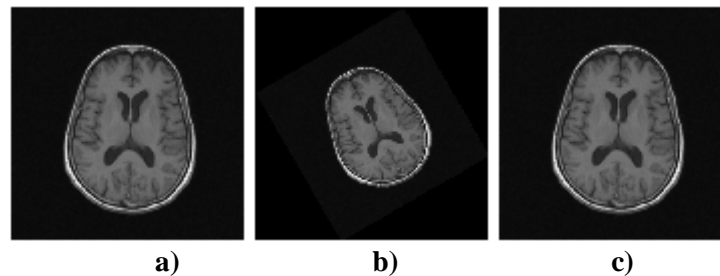


Figure II.13 landmark based registration applied to MRI slice. **a)** reference image, **b)** target image, **c)** registered image

We used six pairs of control points to registrate this image which are:

```
base_points = [200.52 110.32; 135.68 170.12; 107.66 233.22; 193.99 229.12;
```

```
178.96 207.93; 135.68 199.73]
```

```
input_points = [136.37 74.633; 118.9 122.27; 125.96 165.55; 168.1 137.54;
```

```
153.3 130.93; 129.15 140.5].
```

We discovered that if we select a bigger number of control points, the error is minimized.

At first we have applied a deformation to the reference image using the initial parameters mentioned in the table, the result is shown in figure II.13(b), then linear conformal registration is applied to get the result shown in figureII.13.(c), finally, the recovered parameters and the error are calculated and shown in tableII.2

Table II.2 Landmarks based registration results

Initial parameters	Transformation matrix	Recovered parameters	Error
Translation=0 Rotation =30 Scale=0.6	T=[0.52287,-0.29426,0 ; 0.29426,0.52287,0 ;0.24998,76.399,1]	Translation=0 Rotation=29.3699 Scale=0.6000	$FRE^2=31.8820$

This method of registration is good for recovery application, the disadvantage of this method is the manual selection of control points, and testing them many times until minimization of the error (convergence), this is why we have implemented an intensity based registration method.







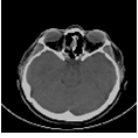
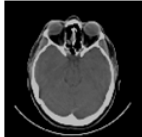
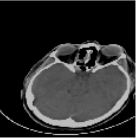
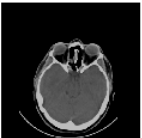
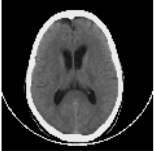
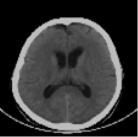
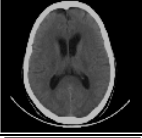

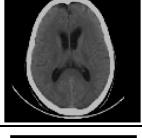
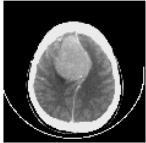

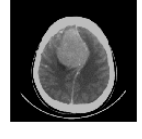
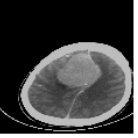
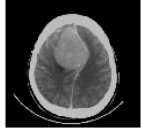
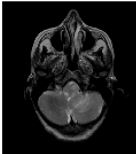
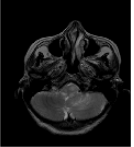
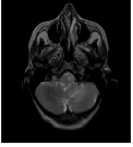
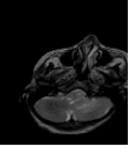
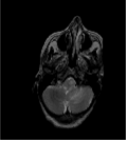
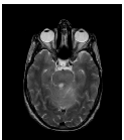
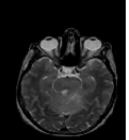
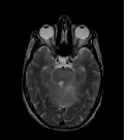
II.6.2 CT/CT and MRI/MRI (Monomodal) registration using CC optimization

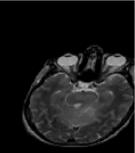
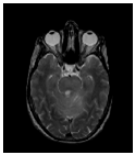
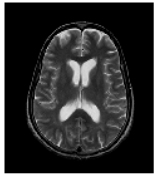
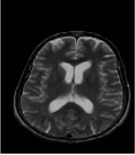
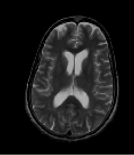
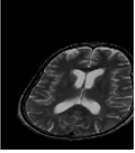
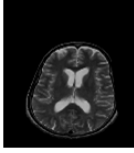
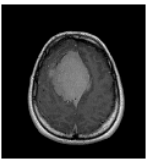
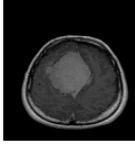
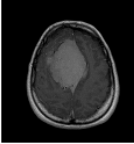
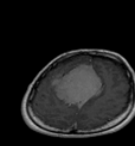
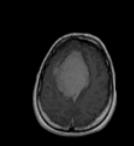

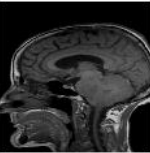

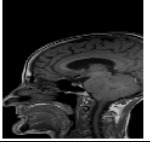
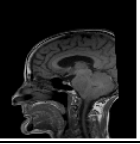
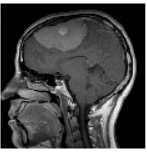
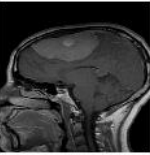
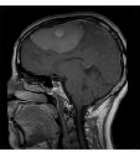
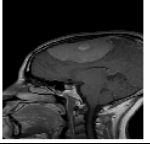
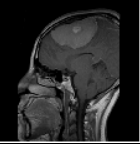
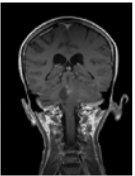
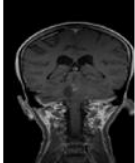
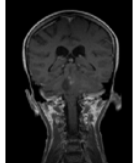
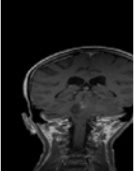
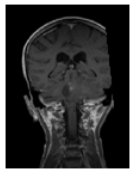
Intensity values of images can also be used as a basis of image registration. The matching is based on direct comparison of pixels scalar values, without need of interaction from the user. The transformation matrix is found by optimizing iteratively a similarity measure. The choice of similarity measure depends on the type of the images used, e.g. we should choose different similarity measure, if would like register MR brain images.

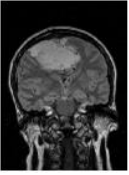
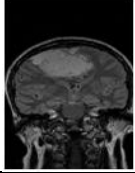

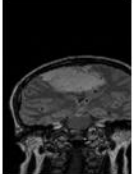
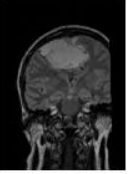
TableII.3 shows the results of the intensity based registration implemented for monomodal images (CT/MRI) for the same patient, the four types of registration are used. The similarity used here is correlation coefficient. The optimization algorithm uses the simplex search method [51]. The user enters only the reference and target image and the algorithm calculates and minimizes the error until convergence.

From our results, we notice that our algorithm converges if the deformation between the reference and target image is not very remarkable as shown in table II.3.

Table II.3 Monomodal intensity based registration results

Slice Number	Original Image	Deformed Image	Recovered Image	Correlation Coefficient
1				0.9761.
				0.6872.
2				0.9738.
				0.5572.
3				0.9817 .
				0.9802.
4				0.9311.
				0.9806.
5				0.9990.
				0.5280.
6				0.9994.

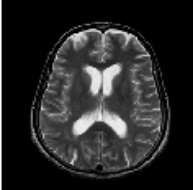
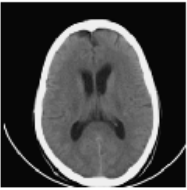
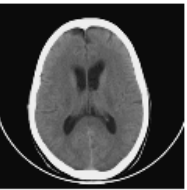
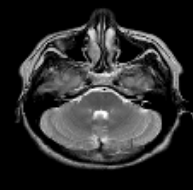
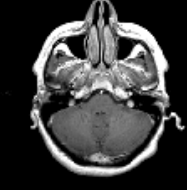
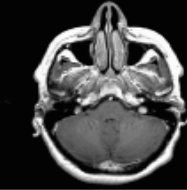
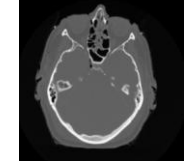
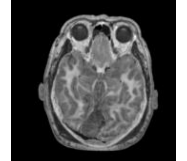
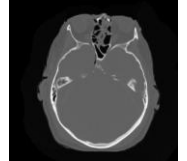
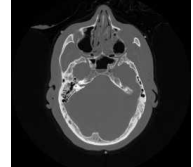
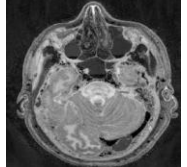
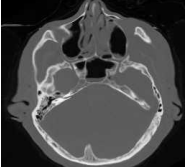
				0.9940.
7				0.7385.
				0.4870.
8				0.9997.
				0.7308.
9				0.9371.
				0.4442.
10				0.9565.
				0.5176.
11				0.9928.
				0.8203.

12				0.9930.
				0.6653.

II.6.3 CT/MRI (multimodal) registration using MI optimization

Table II.4 shows the results of the intensity based registration implemented for multimodal images (CT/MRI) for the same patient, the four types of registration are used. The similarity used here is mutual information. The optimization algorithm uses the simplex search method [51]. The user enters only the reference and target image and the algorithm calculates and minimizes the error until convergence, there is no need to the interaction of the user.

Table II.4 Multimodal intensity based registration

Slice number	MRI (Reference) Image	CT (Float) Image	Registered CT Image	Maximized MI
1				1.1212
2				1.0121
3				1.6515
4				1.6660

II.7. Conclusion

In this chapter the different registration methods in the medical field which have several applications as monitoring changes over time and combining information from multiple imaging modalities have been presented. The classification of these methods is based on many criteria which are dimensionality, transformation, domain of transformation, interaction, optimization, modalities involved in the registration, subject and finally object.

The goal of this work is to select a method able to register images of the brain. A registration method for monomodal and multimodal images which are suitable to register images containing structures of different rigidities. Three methods of registration based on similarity criterion have been implemented, the first method is landmark based registration which is an interactive method and needs the interaction of the user, the fiducial registration error is used as criterion. The second registration method uses the coefficient correlation for monomodal registration. The last registration method uses the mutual information criterion. The intensity based registration method implemented is automatic and doesn't need the interaction of the user.

The discussed methods will be used in the next chapter in fusing techniques from different modalities in the medical field.



Medical Image Fusion

This chapter deals with the medical image fusion which has been used to derive useful information from multi-modality medical image data. Fusion using logical operators, fusion using pseudo color map, and finally fusion using Clustering algorithm are implemented.

III.1 Introduction

Image fusion is the process of combining relevant information from two or more images into a single image to enhance viewing or understanding of the scene [52]. If the images are registered, information can be combined at pixel level. If the images are not registered, information from images should be determined individually and then combined. In this chapter, discussions will be limited to fusion of registered images [24].

The aim of image fusion techniques is to combine and preserve all important visual information obtained from many input images in a single output image. In many applications, the quality of the fused images is very important and is usually assessed by visual analysis subjective to the interpreter. Many quality metrics exist in image fusion, but when no clearly defined ground truth exists, we must construct an ideal fused image to use as a reference for comparing with the experimental results.

III.2 Medical Image Fusion

Imaging the same parts of human anatomy with the different modalities, or with the same modality taken at different times, provides the experts with a great amount of information, which must be combined in order to become diagnostically useful. Medical image fusion is a process that combines information from different images, so its diagnostic value is maximized. [53]

Although much attention has been taken to the process of medical image registration, medical image fusion, as a prerequisite of the process of image registration, is not extensively explored in the literature, mainly because it is considered a straightforward step [53]. A generic approach of the medical image fusion is shown in Figure III.1.

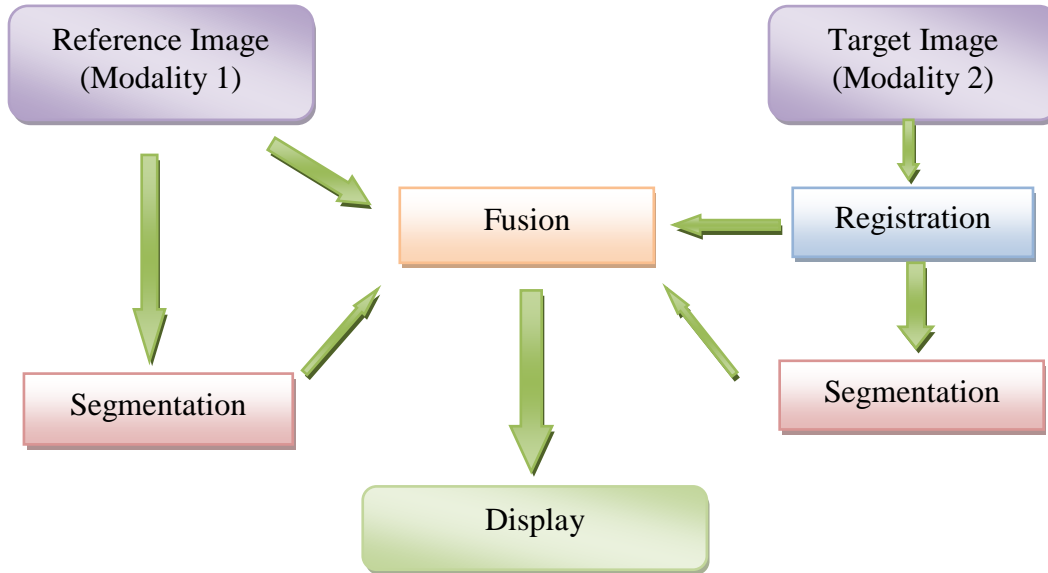


Figure III.1: Generic Medical Image Fusion Scheme.

The most representative techniques reported, will be renewed and broadened to include several methods to combine diagnostic information.

III.2.1 Fusion Using Logical Operators

According to this fusion technique, the reference image, which is not processed, accommodates a segmented region of interest from the second registered image. The simplest way to combine such information from the two images is by using a logical operator such as the XOR operator, according to the following equation [53]:

$$I(x, y) = I_A(x, y)(1 - M(x, y)) + I_B(x, y)M(x, y) \quad (\text{III. 1})$$

where $M(x, y)$ is a Boolean mask that marks with 1s every pixel, which is taken from image B to the fused image $I(x, y)$.

It is desirable in certain cases, to simply delineate the outline of the object of interest from the registered image and to position it in the coordinate system of the reference image. An example of this technique is the extraction of the boundary of an object of interest, such as a tumor from a MR image and overlay it on the coordinate system of the registered CT image of the same patient [99, 100, 101]. Figure III.2 demonstrates the fusion technique using the logical operators on the same patient data,

where CT information (bone structure) is superimposed on two registered MR transverse slices.

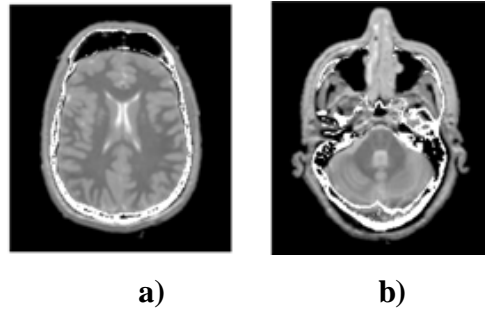


Figure III.2 Fused images using the XOR operator: **a)** CT information (bone structures), **b)** superimposed on two registered MR transverse slices. [53]

III.2.2 Fusion Using a Pseudocolor Map

In the technique of fusing information from two images, the registered image is rendered using a pseudocolor scale and is transparently overlaid on the reference image [54]. There is a number of pseudocolor maps available, defined algorithmically or by using psychophysiologic criteria. A pseudocolor map is defined as a correspondence of an (R, G, B) triplet to each distinct pixel value. Usually, the pixel value ranges from 0 to 255, and each of the elements of the triplet varies in the same range, thus producing a true color effect. The color map is called “pseudo” because only one value is acquired for each pixel during the acquisition of the image data.

Two of the pseudocolor maps that are defined by psychophysiologic criteria are the geographic color map and the hot body color map. The (R, G, B) triplet values are defined as a function of the original pixel value according to the following equation:

$$(R, G, B) = (R(\text{pixel}_{\text{value}}), G(\text{pixel}_{\text{value}}), B(\text{pixel}_{\text{value}})) \quad (\text{III. 2})$$

The RGB Cube color map is a positional color map, which maps the original values to a set of colors that are determined by traversing the following edges of a cube:

$$\begin{aligned} B(0, 0, 1) &\rightarrow (1, 0, 1) \rightarrow R(1, 0, 0) \rightarrow (1, 1, 0) \rightarrow G(0, 1, 0) \rightarrow (0, 1, 1) \\ &\rightarrow B(0, 0, 1) \end{aligned} \quad (\text{III. 3})$$

This configuration sets up six color ranges, each of which has $N/6$ steps, where N is the number of colors (distinct pixel values) of the initial image. If N is not a factor of 6, the difference is made up at the sixth range. The CIE Diagram color map follows the same philosophy, thus traversing a triangle on the RGB *Cube* in the following manner:

$$R(1, 0, 0) \rightarrow G(0, 1, 0) \rightarrow B(0, 0, 1) \quad (\text{III. 4})$$

Another useful color map for biomedical images is the Gray Code. This color map is constructed by a three-bit gray code, where each successive value differs by a single bit. A number of additional color maps, such as HSV Rings and Rainbow, are constructed by manipulating the color in the HSV coordinate system (Hue/Saturation/Value coordinate system). The conversion from HSV to RGB is straightforward [53].

Figures III.3, III.4 show an example of RGB pseudocolor map of a CT and MRI images.

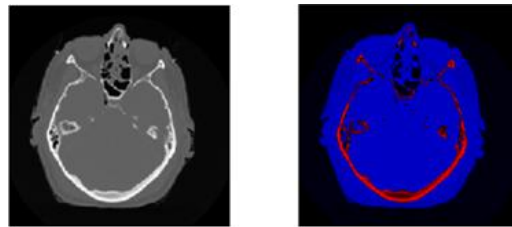


Figure III.3 RGB Cube pseudocolor map of CT image

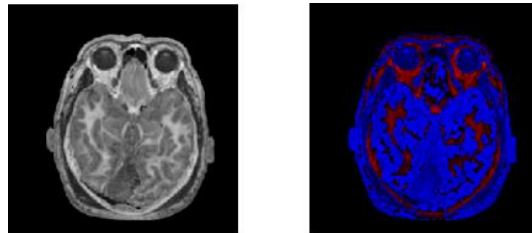


Figure III.4 RGB Cube pseudocolor map of MRI image

III.2.3 Clustering Algorithms for Unsupervised Fusion of Registered Images

Data fusion on the image level can be achieved by processing both registered images in order to produce a fused image with an appropriate pixel classification. The key quantity in this technique is the histogram of the two registered images. Fusing the registered images to produce an enhanced or segmented/classified image becomes equivalent to partitioning the histogram to a desired number of classes using a clustering algorithm. The goal of clustering is to reduce the amount of data by categorizing similar data items together. Such grouping is pervasive in the way humans process information. Clustering is used to provide an automatic tool for constricting categories in data feature space. Clustering algorithms can be divided into two basic types such as hierarchical and partitional [55]. Hierarchical algorithms are initialized by a random definition of clusters

and evolve by splitting large inhomogeneous clusters or merging small similar clusters. Partitional algorithms attempt to directly decompose the data into a set of disjoint clusters by minimizing a measure of dissimilarity between data points in the same clusters, while maximizing dissimilarity between data points in different clusters.

III.2.3.1. The Kmeans Algorithm

K-means clustering is a method of cluster analysis which aims to partition n observations into k clusters in which each observation belongs to the cluster with the nearest mean. It is similar to the expectation-maximization algorithm for mixtures of Gaussians in that they both attempt to find the centers of natural clusters in the data [56].

The K-means algorithm is a partitional clustering algorithm, which is used to distribute points in feature space among a predefined number of classes [57].

In k-means clustering each point is assigned to the cluster whose center (also called centroid) is nearest. The center is the average of all the points in the cluster that is, its coordinates are the arithmetic mean for each dimension separately over all the points in the cluster [58].

The K-means algorithm is the most famous and most used clustering algorithm due to its simplicity of implementation and also its speed. When it is applied to an image, it takes a number of clusters (classes of regions) defined manually and attempts to group the pixels into the given number of clusters. The algorithm begins with some K initial centers m_i that can be provided manually or generated randomly [59]. Each pixel is assigned to the closest center, based on some measure that we will define as distance. Each center is then recalculated to be the average of every pixel assigned to its cluster. The algorithm then iteratively repeats until convergence, which is guaranteed.

The algorithm which is applied in pseudocode can be summarized as follows: [58, 60, 61]

1. Choose the number of clusters, k .
2. Randomly generate k clusters and determine the cluster centroids m_k (centers of each class), or directly generate k random points as cluster centers.
3. Assign each point S to the nearest cluster centroids.

$$C(s) = \operatorname{argmin} \|y_s - m_k\|^2, S = 1, \dots, N \quad (\text{III. 5})$$

Where $C(s)$: is the class to which the pixel is assigned and Y_s : grey level of the pixel s

4. Recompute the new cluster centroids.

$$m_i = \frac{\sum_{j:N_i} x_j}{N_i}, i = 1, \dots, K \quad (\text{III.6})$$

5. Repeat the two previous steps until some convergence criterion is met (usually that the assignment hasn't changed).

The steps of the algorithm; are summarized as shown in figure III.4 where the k-means clustering method is applied on a set of randomly generated points [56, 62]:

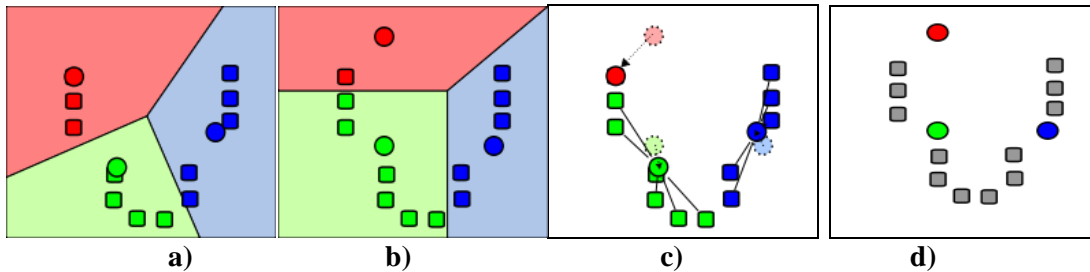


Figure III.5 k-means clustering method applied on a set of randomly generated points.

- a) k initial "means" (in this case $k=3$) are randomly selected from the data set (shown in color),
- b) k clusters are created by associating every observation with the nearest mean. The partitions here represent the Voronoi diagram generated by the means,
- c) The centroid of each of the k clusters becomes the new means,
- d) Steps 2 and 3 are repeated until convergence has been reached.

The above algorithm can be employed to utilize information from pairs of images, such as CT, SPECT, MRI-T1, MRI-T2, and functional MRI, to achieve tissue classification and fusion. For tissue classification, nine different classes are usually sufficient, corresponding to background, cerebrospinal fluid, gray and white matter, bone material, abnormalities, etc. If fusion is required, then 64 or more classes can be defined, providing enhancement of the fine details of the original images. In Figure III.6, a fused image using the K-means algorithm for different classes of tissue is produced by fusing CT and MR images of the same patient.

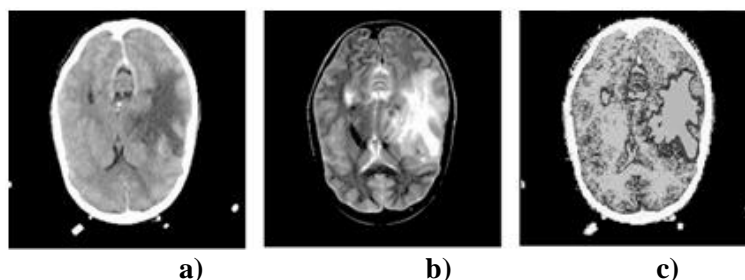


Figure III.6 Fused image using the K -means algorithm for different classes of tissue: a) reference CT image, b) registered MRI image of the same patient, and c) fusion result [53].

K-means algorithm may be used to segment medical images that present a fairly uniform grey level. We present the overall pixels by a one dimensional space based on their grey level, we obtain a cloud of points on which we apply K-means algorithm just like what was shown above.

The K-means algorithm has been applied to a set of CT and MRI slices. As shown in figure III.7 and figure III.11, it is applied on MRI and CT slices containing the tumor, it demonstrates the detection of the tumor (abnormal tissue recognition), where (a) represents the original image, (b) is the results of the original image after applying the k-means algorithm, the image is segmented on three classes as it is shown, then a separation of the three different clusters is done as shown in (c) brain matter, (d) tumor class, and finally the skull in (e).

The figure III.8 shows the normal tissue recognition of MRI slice where (a) is the original image, (b) is the result image after clustering, three clusters are defined which are the white matter, the gray matter and the CSF shown in (c), (d) and (e) respectively.

The figures III.9 and III.10 shows the results of k-means clustering applied on CT and MRI slices respectively. These images contains only two classes which are the brain matter (also called intracranial area) and the bone structure (skull)

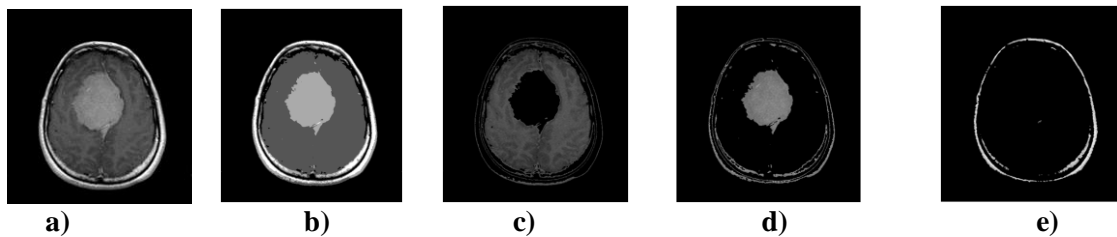


Figure III.7 k-means algorithm applied on MRI slice (3 classes in this case)
 a) Original MRI slice, b) Clustered MRI slice, c) Objects in cluster 1, d) Objects in cluster 2,
 e) Objects in cluster 3

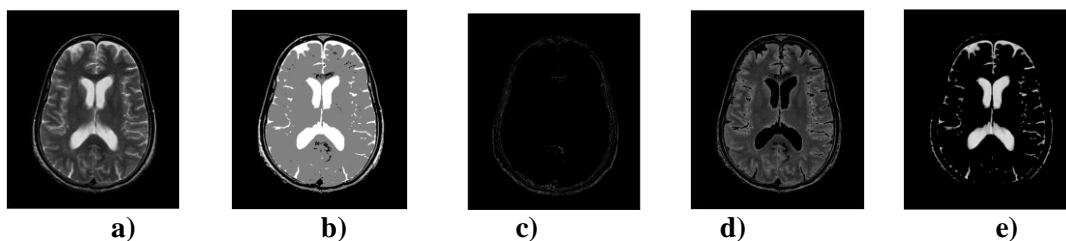


Figure III.8 k-means algorithm applied on MRI slice (3 classes in this case)
 a) Original MRI slice, b) Clustered MRI slice, c) Objects in cluster 1, d) Objects in cluster 2,
 e) Objects in cluster 3

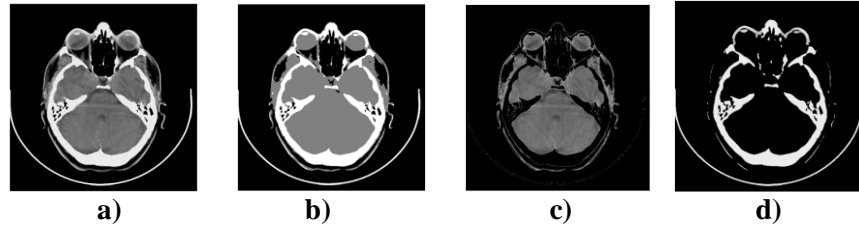


Figure III.9 k-means algorithm applied on CT slice (2 classes in this case)
 a) Original CT slice, b) Clustering CT slice, c) Objects in cluster 1, d) Objects in cluster 2.

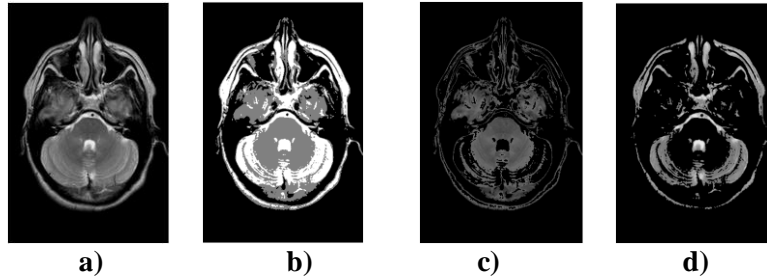


Figure III.10 k-means algorithm applied on MRI slice (2 classes in this case)
 a) Original MRI slice, b) Clustering MRI slice, c) Objects in cluster 1, d) Objects in cluster 2.

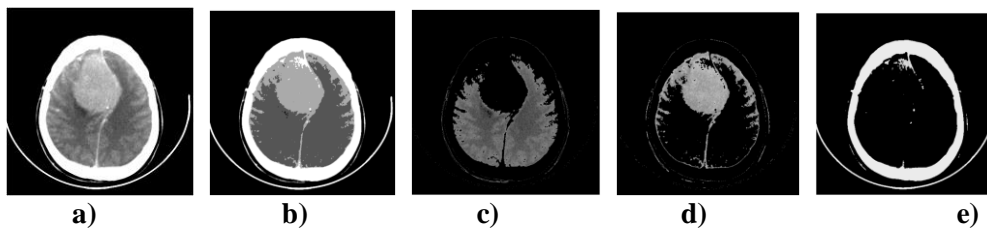


Figure III.11 k-means algorithm applied on CT slice (3 classes in this case)
 a) Original CT slice, b) Clustering CT slice, c) Objects in cluster 1, d) Objects in cluster 2,
 e) Objects in cluster 3

The main advantages of this algorithm are its simplicity and speed which allows it to run on large datasets. Its disadvantage is that it does not yield the same result with each run, since the resulting clusters depend on the initial random assignments. It minimizes intra-cluster variance, but does not ensure that the result has a global minimum of variance. Another disadvantage is the requirement for the concept of a mean to be definable which is not always the case [58].

III.2.3.2 The Fuzzy Kmeans Algorithm

The Fuzzy K-Means algorithm also called Fuzzy C-Means algorithm is an extension of K-Means [54], the popular simple clustering technique. While K-Means discovers hard clusters (a point belong to only one cluster), Fuzzy K-Means is a more statistically formalized method and discovers soft clusters where a particular point can

belong to more than one cluster with certain probability. It is a method of clustering which allows one piece of data to belong to two or more clusters. It is a variation of the K-means algorithm, with the introduction of fuzziness in the form of a membership function. The membership function defines the probability with which each image pixel belongs to a specific class.

The membership function assigns to a data point x a positive, less than or equal to one, probability u_{jx} which indicates that point x belongs to class j . To meet computational requirements, the membership function is implemented as a 2-D matrix, where first index indicates the cluster and the second index indicates the value of the data point. If the membership function is to express mathematical probability, the following constraint applies [98]:

$$\sum_{i=1}^n u_{ij} = 1, \quad \forall \text{ cluster } j \quad (\text{III. 7})$$

This method is based on minimization of the following objective function:

$$E = \sum_{j=1}^k \sum_{i=1}^n u_{ij}^p \|x_i - m_j\|^2, \quad 1 \leq p < \infty \quad (\text{III. 8})$$

where the exponential p is a real number greater than 1 and controls the fuzziness of the clustering process.

where m is any real number greater than 1, u_{ij} is the degree of membership of x_i in the cluster j , x_i is the i^{th} of d -dimensional measured data, m_j is the d -dimension center of the cluster, and $\|\cdot\|$ is any norm expressing the similarity between any measured data and the center.

Fuzzy partitioning is carried out through an iterative optimization of the objective function shown above, with the update of membership u_{ij} and the cluster centers m_j by:

$$m_j = \frac{\sum_{i=1}^N u_{ij}^p x_i}{\sum_{i=1}^N u_{ij}^p}, \quad j = 1, \dots, k \quad (\text{III. 9})$$

$$u_{ij} = \left(\sum_{k=1}^m \left(\frac{\|x_i - m_j\|}{\|x_i - m_k\|} \right)^{\frac{2}{p-1}} \right)^{-1} \quad (\text{III. 10})$$

This iteration will stop when $\max\{|u_{ij}(k+1) - u_{ij}(k)|\} < \varepsilon$, where ε is a termination criterion between 0 and 1, whereas k are the iteration steps. This procedure converges to a local minimum or a saddle point of E . The algorithm is composed of the following steps [57, 63, 64]:

1. Initialize $U = [u_{ij}]$ matrix, $U(0)$.
2. At k -step: calculate the centers vectors $\mathbf{m}(k) = [m_j]$ with $U(k)$ using equation (III.9).
3. Update $U(k)$, $U(k+1)$ using equation (III.10).
4. If $\|U(k+1) - U(k)\| < \varepsilon$ then STOP; otherwise return to step 2.

The algorithm minimizes intra-cluster variance as well, but has the same problems as k -means, the minimum is a local minimum, and the results depend on the initial choice of weights. The expectation-maximization algorithm is a more statistically formalized method which includes some of these ideas: partial membership in classes. It has better convergence properties and is in general preferred to fuzzy-c-means [58, 65].

The fuzzy K-means algorithm has been applied to a set of CT and MRI slices containing the tumor as shown in figure III.12 and figure III.13 respectively, it demonstrates the detection of the tumor (abnormal tissue recognition), where (a) represents the original image, (b) is the results of the original image after applying the fuzzy k-means algorithm, the image is segmented on three classes as it is shown, then a separation of the three different clusters is done as shown in (c) brain matter, (d) tumor class, and finally the skull in (e).

The figure III.16 shows the normal tissue recognition of MRI slice where (a) is the original image, (b) is the result image after clustering, three clusters are defined which are the white matter, the gray matter and the CSF shown in (c), (d) and (e) respectively.

The figures III.14 and III.15 shows the results of fuzzy k-means clustering applied on MRI and CT slices respectively. These images contain only two classes which are the brain matter (also called intracranial area) and the bone structure (skull).

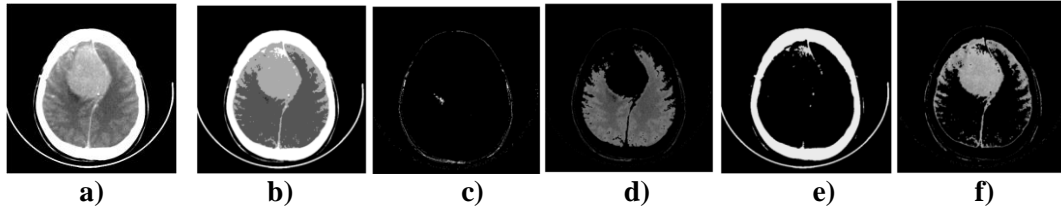


Figure III.12 Fuzzy k-means algorithm applied on CT slice. **a)** Original CT slice, **b)** Clustered CT slice, **c)** Objects in cluster 1, **d)** Objects in cluster 2, **e)** Objects in cluster 3, **f)** Objects in cluster 4.

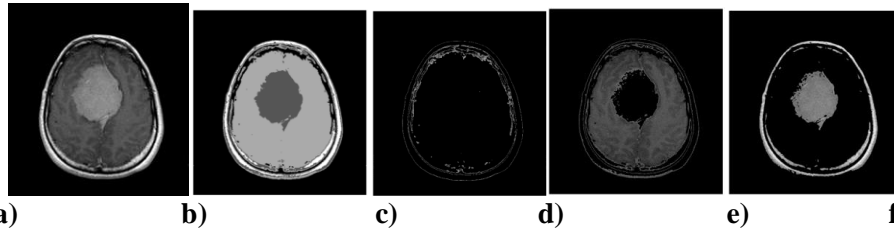


Figure III.13 Fuzzy k-means algorithm applied on MRI slice. **a)** Original MRI slice, **b)** Clustered MRI slice, **c)** Objects in cluster 1, **d)** Objects in cluster 2, **e)** Objects in cluster 3, **f)** Objects in cluster 4.

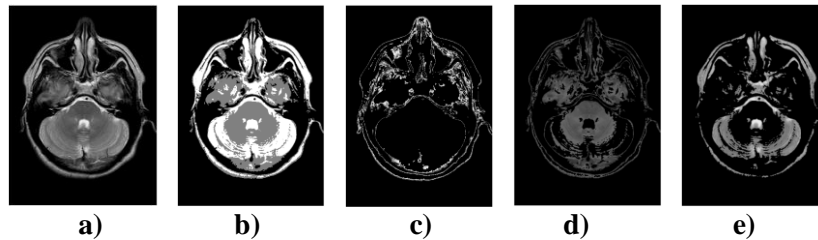


Figure III.14 Fuzzy k-means algorithm applied on MRI slice. **a)** Original MRI slice, **b)** Clustered MRI slice, **c)** Objects in cluster 1, **d)** Objects in cluster 2, **e)** Objects in cluster 3.

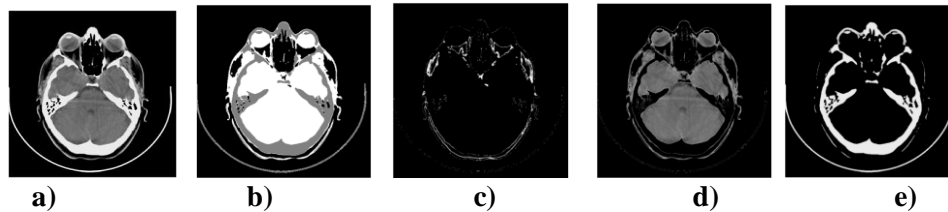


Figure III.15 Fuzzy k-means algorithm applied on CT slice. **a)** Original CT slice, **b)** Clustered CT slice, **c)** Objects in cluster 1, **d)** Objects in cluster 2, **e)** Objects in cluster 3.

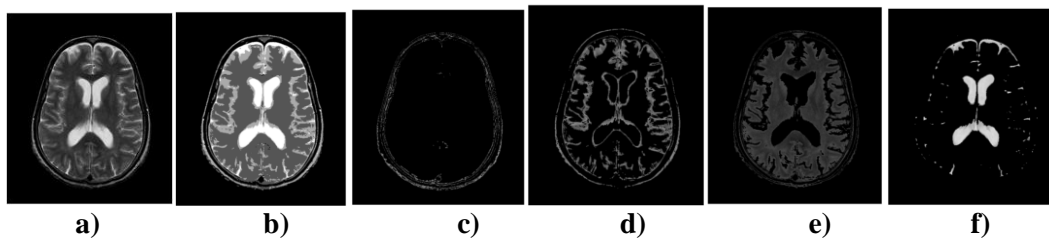


Figure III.16 Fuzzy k-means algorithm applied on MRI slice. **a)** Original MRI slice, **b)** Clustered MRI slice, **c)** Objects in cluster 1, **d)** Objects in cluster 2, **e)** Objects in cluster 3, **f)** Objects in cluster 4.

III.2.3.4 Threshold algorithm

a. Global threshold

During the thresholding process, bright pixels in an image are considered as object pixels and others are considered as “background” pixels, if their value is greater than some threshold value (assuming an object to be brighter than the background). It is known as threshold. Variants include threshold below, which is opposite of threshold above; threshold inside, where a pixel is labeled object if its value is between two thresholds; and threshold outside, which is the opposite of threshold inside [66]. Typically, an object pixel is given by a value of “1” while a background pixel is given by a value of “0”. Finally, a binary image is created by coloring each pixel white or black, depending on a pixel's label [67].

Thresholding creates binary images from grey-level ones by turning all pixels below some threshold to zero and all pixels about that threshold to one. (What you want to do with pixels at the threshold doesn't matter, as long as you're consistent.)

If $g(x, y)$ is a thresholded version of $f(x, y)$ at some global threshold T ,

$$g(x, y) = \begin{cases} 1 & \text{if } f(x, y) \geq T \\ 0 & \text{elsewhere} \end{cases} \quad (\text{III. 11})$$

Threshold selection

The key parameter in the thresholding process is the choice of the threshold value (or values, as mentioned earlier). Different methods for choosing a threshold can be used. Users can manually choose a threshold value, or a thresholding algorithm can compute a value automatically, which is known as automatic thresholding [66]. A simple method would be to choose the mean or median value, the rationale being that if the object pixels are brighter than the background, they should also be brighter than the average. In a noiseless image with uniform background and object values, the mean or median will work well as the threshold, however, this will generally not be the case. A more sophisticated approach might be to create a histogram of the image pixel intensities and use the valley point as the threshold. The histogram approach assumes that there is some average value for the background and object pixels, but that the actual pixel values have some variation around these average values. However, this may be computationally expensive, and image histograms may not have clearly defined valley points, often

making the selection of an accurate threshold difficult. One method that is relatively simple, does not require much specific knowledge of the image, and is robust against image noise, is the following iterative method [67]:

1. An initial threshold (T) is chosen, this can be done randomly or according to any other method desired.
2. The image is segmented into object and background pixels as described above, creating two sets:

$$\bullet G_1 = \{f(m, n): f(m, n) > T\} \quad (\text{III. 12})$$

Object pixels.

$$\bullet G_2 = \{f(m, n): f(m, n) \leq T\} \quad (\text{III. 13})$$

Background pixels, it can be noted that $f(m, n)$ is the value of the pixel located at the m^{th} column, n^{th} row.

3. The average of each set is computed.

$$\bullet m_1 = \text{average value of } G_1 \quad (\text{III. 14})$$

$$\bullet m_2 = \text{average value of } G_2 \quad (\text{III. 15})$$

4. A new threshold is created that is the average of m_1 and m_2

$$\bullet T' = (m_1 + m_2)/2 \quad (\text{III. 16})$$

5. Go back to step two, now using the new threshold computed in step four, keep repeating until the new threshold matches the one before it (i.e. until convergence has been reached).

This iterative algorithm is a special one-dimensional case of the k-means clustering algorithm, which has been proven to converge at a local minimum meaning that a different initial threshold may give a different final result.

Problems with Thresholding

The major problem with thresholding is that we consider only the intensity, not any relationships between the pixels. There is no guarantee that the pixels identified by the thresholding process are contiguous.

We can easily include extraneous pixels that aren't part of the desired region, and we can just as easily miss isolated pixels within the region (especially near the boundaries of the region). These effects get worse as the noise gets worse, simply because it's more likely

that a pixels intensity doesn't represent the normal intensity in the region. When we use thresholding, we typically have to play with it, sometimes losing too much of the region and sometimes getting too many extraneous background pixels. Shadows of objects in the image are also a real pain not just where they fall across another object but where they mistakenly get included as part of a dark object on a light background [68].

b. Local Threshold

Another problem with global thresholding is that changes in illumination across the scene may cause some parts to be brighter (in the light) and some parts darker (in shadow) in ways that have nothing to do with the objects in the image.

We can deal, at least in part, with such uneven illumination by determining thresholds locally. That is, instead of having a single global threshold, we allow the threshold itself to smoothly vary across the image.

Thresholding is called adaptive thresholding when a different threshold is used for different regions in the image. This may also be known as local or dynamic thresholding [69]. The results of the global threshold algorithm applied to a set of CT and MRI slices are shown in figure III.17 and figure III.18:

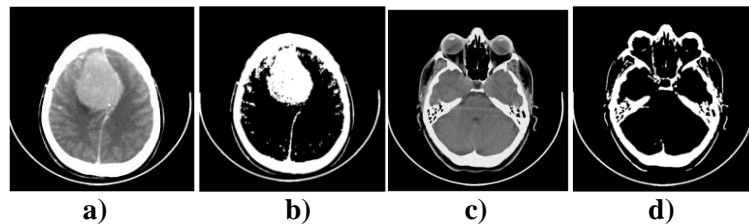


Figure III.17 Thresholding algorithm applied to CT slice. **a)** original image, **b)** thresholded image, **c)** original image, **d)** thresholded image.

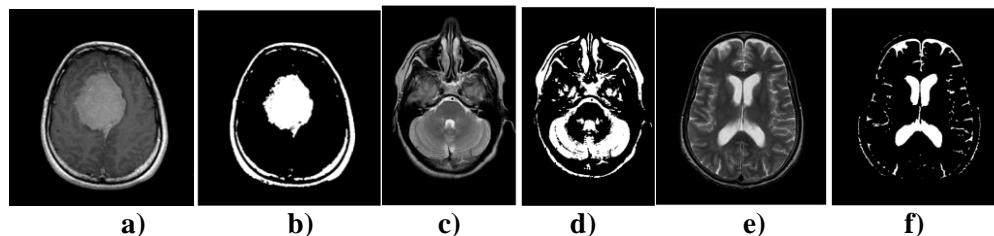


Figure III.18 Thresholding algorithm applied to MRI slice. **a)** original image, **b)** thresholded image, **c)** original image, **d)** thresholded image, **e)** original image, **f)** thresholded image.

c. Otsu's method

Otsu's method is used to automatically perform histogram shape-based thresholding, or, the reduction of a gray level image to a binary image. The algorithm assumes that the image to be thresholded contains two classes of pixels, object and background, then calculates the optimum threshold separating those two classes so that their combined spread (intra-class variance) is minimal. The extension of the original method to multi-level thresholding is referred to as the Multi Otsu method [70]. Another way of accomplishing similar results is to set the threshold so as to try to make each cluster as tight as possible, thus (hopefully!) minimizing their overlap. Obviously, we can't change the distributions, but we can adjust where we separate them (the threshold). As we adjust the threshold one way, we increase the spread of one and decrease the spread of the other. The goal then is to select the threshold that minimizes the combined spread [68].

Otsu's method uses a quite different way to choose the threshold value. Its actually based on a very simple idea: find the threshold that minimizes the weight with-in class variance which turns out to be the same as maximizing the between class variance. What makes Otsu's method as popular as it is, is the fact that operates directly on the grey level histogram, so it is fast (once the histogram is computed) [54].

Algorithm

In Otsu's method we exhaustively search for the threshold that minimizes the intra-class variance, defined as a weighted sum of variances of the two classes:

$$\sigma_w^2(t) = q_1(t)\sigma_1^2(t) + q_2(t)\sigma_2^2(t) \quad (\text{III. 17})$$

Weights q_i are the probabilities of the two classes separated by a threshold t and σ_i^2 variances of these classes.

$\sigma_1^2(T) =$ the variance of the pixels in the background (below threshold),

$\sigma_2^2(T) =$ the variance of the pixels in the foreground (above threshold),

$$q_1(t) = \sum_{i=1}^t P(i) \quad (\text{III. 18})$$

$$q_2(t) = \sum_{i=t+1}^I P(i) \quad (\text{III. 19})$$

And the class means are given by:

$$\mu_1(t) = \sum_{i=1}^t \frac{iP(i)}{q_1(t)} \quad (\text{III. 20})$$

$$\mu_2(t) = \sum_{i=t+1}^I \frac{iP(i)}{q_2(t)} \quad (\text{III. 21})$$

Finally, the individual class variances are:

$$\sigma_1^2(t) = \sum_{i=1}^t [i - \mu_1(t)]^2 \frac{P(i)}{q_1(t)} \quad (\text{III. 22})$$

$$\sigma_2^2(t) = \sum_{i=t+1}^I [i - \mu_2(t)]^2 \frac{P(i)}{q_2(t)} \quad (\text{III. 23})$$

Otsu shows that minimizing the intra-class variance is the same as maximizing inter-class variance:

$$\sigma_{Between}^2(T) = \sigma^2 - \sigma_{Within}^2(T) \quad (\text{III. 24})$$

which is expressed in terms of class probabilities q_i and class means μ_i which in turn can be updated iteratively. This idea yields an effective algorithm.

So, for each potential threshold T we

1. Separate the pixels into two clusters according to the threshold.
2. Find the mean of each cluster.
3. Square the difference between the means.
4. Multiply by the number of pixels in one cluster times the number in the other.

This depends only on the difference between the means of the two clusters, thus avoiding having to calculate differences between individual intensities and the cluster means. The optimal threshold is the one that maximizes the between-class variance (or, conversely, minimizes the within-class variance).

This still sounds like a lot of work, since we have to do this for each possible threshold, but it turns out that the computations aren't independent as we change from one threshold to another. We can update $n_B(T)$, $n_0(T)$, and the respective cluster means $\mu_B(T)$ and $\mu_0(T)$ as pixels move from one cluster to the other as T increases.

And the results of the otsu algorithm applied on a set of CT and MRI slices are shown on figure III.19 and III.20:

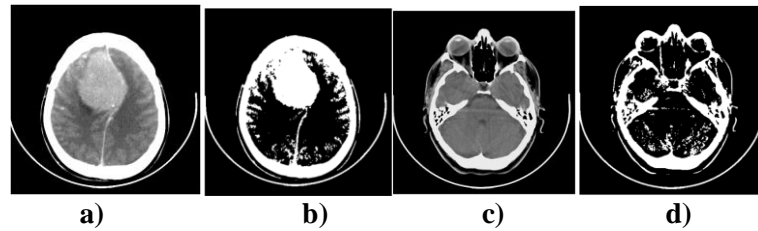


Figure III.19 Otsu's algorithm applied to CT slice. **a)** original image, **b)** thresholded image, **c)** original image, **d)** thresholded image.

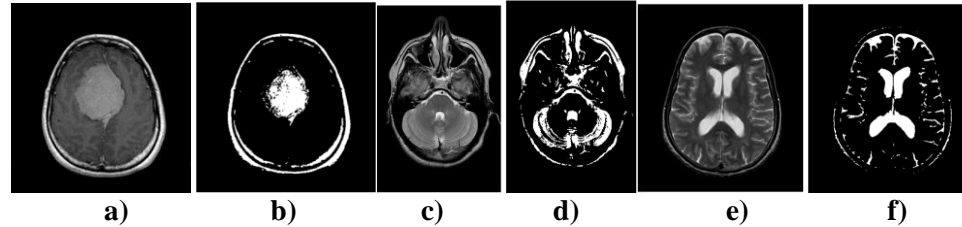


Figure III.20 Otsu's algorithm applied to MRI slice. **a)** original image, **b)** thresholded image, **c)** original image, **d)** thresholded image, **e)** original image, **f)** thresholded image.

III.2.3.4 Brain classification based on EM segmentation

Expectation-maximization is a very popular framework for different classification problems such as in segmentation of brain MRI during last decade. However, it is not easy to understand the underlying theory [71].

Expectation Maximization(EM) is one of the most common algorithms used for density estimation of data points in an unsupervised setting. The algorithm relies on finding the maximum likelihood estimates of parameters when the data model depends on certain latent variables. In EM, alternating steps of Expectation (E) and Maximization (M) are performed iteratively till the results converge. The E step computes an expectation of the likelihood by including the latent variables as if they were observed, and a maximization (M) step, which computes the maximum likelihood estimates of the parameters by maximizing the expected likelihood found on the last E step [72]. The parameters found on the M step are then used to begin another E step, and the process is repeated until convergence [73].

Mathematically for a given training dataset $\{x(1); x(2); \dots x(m)\}$ and model $p(x, z)$ where z is the latent variable, we have:

$$l(\theta) = \sum_{i=1}^m \log p(x, \theta) \quad (\text{III. 25})$$

$$= \sum_{i=1}^m \log \sum_z p(x, z, \theta) \quad (\text{III. 26})$$

It can be noticed from the above equation, The log likelihood is described in terms of x , z and θ . But since z , the latent variable is not known, We use approximations in its place. These approximations take the form of E & M steps mentioned above and formulated mathematically as,

E Step, for each i :

$$Q_i(z^{(i)}) = p(z^{(i)} | x^{(i)}, \theta) \quad (\text{III. 27})$$

M Step, for all z :

$$\theta = \underset{\theta}{\operatorname{argmax}} \sum_i \sum_{z^{(i)}} Q_i(z^{(i)}) \log \frac{p(x^{(i)}, z^{(i)}, \theta)}{Q_i(z^{(i)})} \quad (\text{III. 28})$$

where Q_i is the posterior distribution of $z^{(i)}$'s given the $x^{(i)}$'s.

Conceptually, The EM algorithm can be considered as a variant of the K Means algorithm where the membership of any given point to the clusters is not complete and can be fractional.

Figure III.21, figure III.23, figure III.25, figure III.27 and figure III.29 show the log of the histogram assigned to each following image which is mentioned in blue, the maximum log likelihood in red, and the Gaussian distribution of each class in green.

The EM segmentation algorithm has been applied to a set of CT and MRI slices containing the tumor as shown in figure III.22 and figure III.24 respectively, it demonstrates the detection of the tumor (abnormal tissue recognition), where (a) represents the original image, (b) is the results of the original image after applying the EM segmentation algorithm, the image is segmented on three classes as it is shown, then a separation of the three different clusters is done as shown in (c) brain matter, (d) tumor class, and finally the skull in (e).

The figure III.30 shows the normal tissue recognition of MRI slice where (a) is the original image, (b) is the result image after clustering, three clusters are defined which are the white matter, the gray matter and the CSF shown in (c), (d) and (e) respectively.

The figures III.26 and III.28 shows the results of EM segmentation applied on MRI and CT slices respectively. These images contains only two classes which are the brain matter (also called intracranial area) and the bone structure (skull).

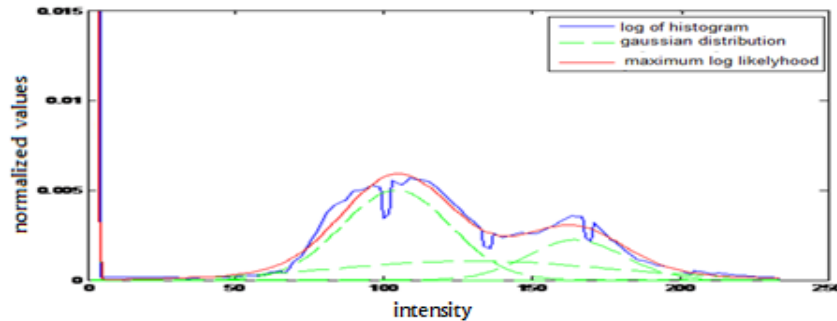


Figure III. log of the histogram, result of maximum log likelihood, and Gaussian distribution of each class.

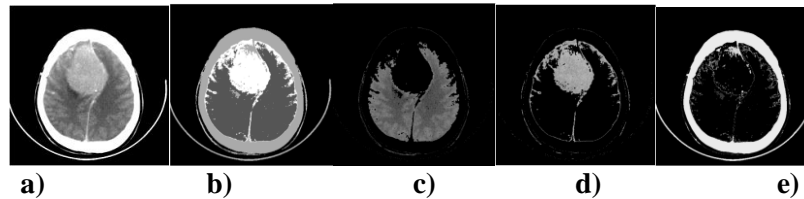


Figure III.22 EM Segmentation algorithm applied to CT slice.

a) Original CT slice, b) Clustered CT slice, c) Objects in cluster 1, d) Objects in cluster 2, e) Objects in cluster 3.

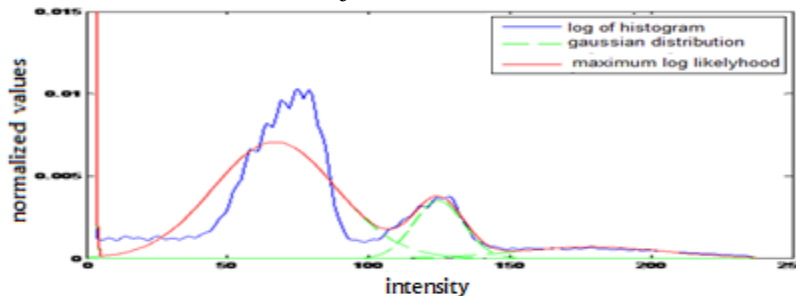


Figure III.23 log of the histogram, result of maximum log likelihood, and Gaussian distribution of each class.

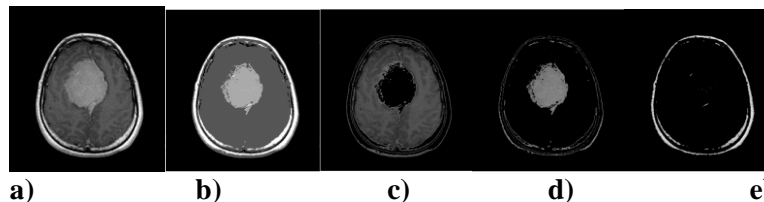


Figure III.24 EM Segmentation algorithm applied on MRI slice.

a) Original MRI slice, b) Clustered MRI slice, c) Objects in cluster 1, d) Objects in cluster 2, e) Objects in cluster 3.

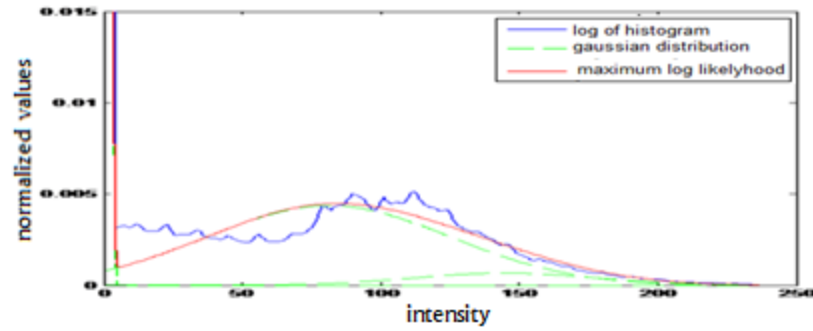


Figure III.25 log of the histogram, result of maximum log likelihood, and Gaussian distribution of each class.

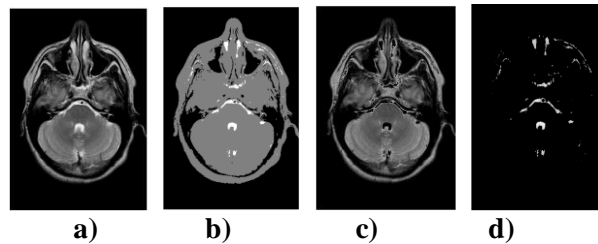


Figure III.26 EM Segmentation algorithm applied on MRI slice.
 a) Original MRI slice, b) Clustered MRI slice, c) Objects in cluster 1, d) Objects in cluster 2,
 e) Objects in cluster 3.

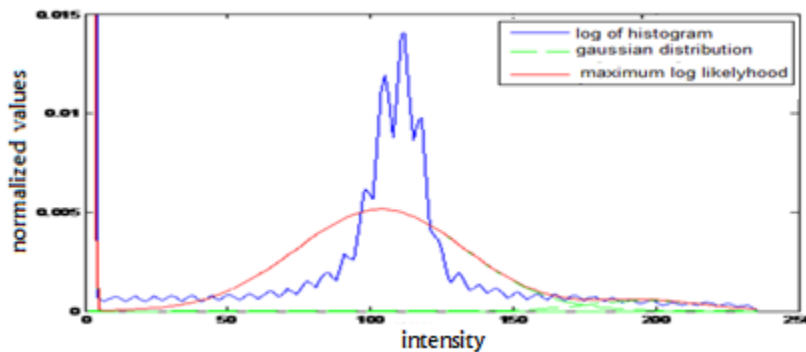


Figure III.27 log of the histogram, result of maximum log likelihood, and Gaussian distribution of each class.



Figure III.28 EM Segmentation algorithm applied on CT slice.
 a) Original CT slice, b) Clustered CT slice, c) Objects in cluster 1, d) Objects in cluster 2,
 e) Objects in cluster 3

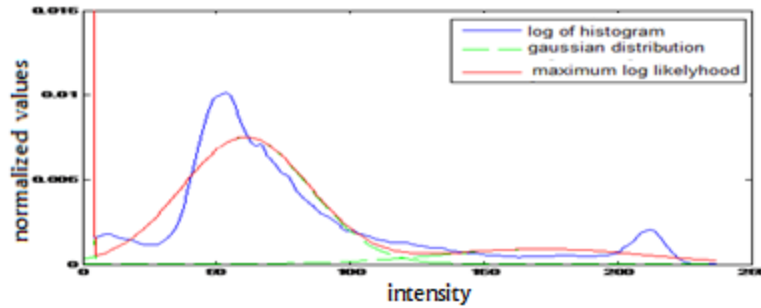


Figure III.29 log of the histogram, result of maximum log likelihood, and Gaussian distribution of each class.

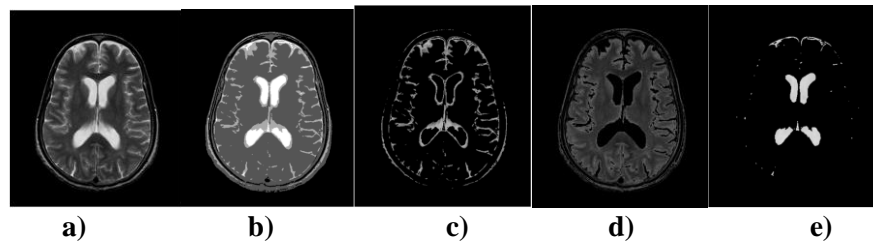


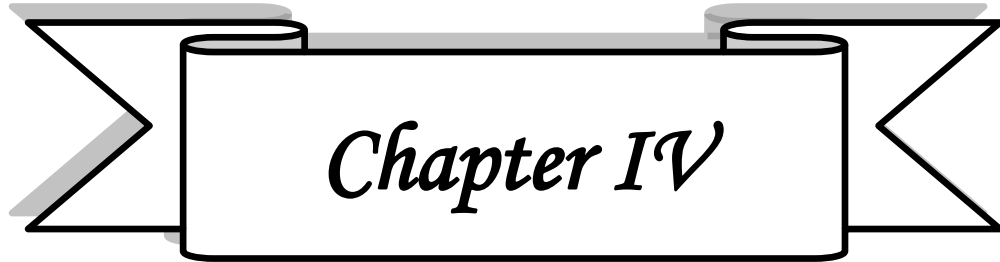
Figure III.30 EM Segmentation algorithm applied on MRI slice.

a) Original MRI slice, b) Clustered MRI slice, c) Objects in cluster 1, d) Objects in cluster 2, e) Objects in cluster 3.

III.3. Conclusion

In this chapter, methods of medical image fusion are presented and implemented, first using logical operators, second using pseudocolor map, and last using the clustering algorithms for unsupervised fusion of registered images. We name the k-means algorithm, the fuzzy k-means algorithm, the EM segmentation and finally the threshold algorithm including the otsu algorithm. From our observation, we discovered that two methods which are k-means and fuzzy k-means clustering can be adopted to identify the potential abnormal regions. EM segmentation is better for normal tissue recognition. Threshold and Otsu can be used for skull extraction.

The aim of the proposed methods is to extract a segmented region of interest from the registered image and then overlay it on the second image. We applied this technique of fusion in certain applications in the medical field which are done in the next chapter, we made also a comparison between the methods of clustering listed before.



Medical Image Registration and Fusion Methods Implementation

In this research, transformation domain image fusion approaches for fusing medical images of two different modalities, CT and MRI have been obtained.

IV .1 Introduction

This chapter deals with a relatively new approach applied to image processing, which has been proved to be of high importance in medical applications, for obtaining qualitatively new data by combining several different images (or sequences of images). The term *image fusion* is used here for a very generic sense of synthesizing the new information based on combining and mutually complementing the information from more than an one image. Although in this work, it may be understood that medical image fusion often concerns three-dimensional image data provided by tomography modalities. However, the three-dimensional fusion is, disregarding rare exceptions, a conceptually simple generalization of the two-dimensional case. The most common and obviously clinically needed is the *image registration* in its many variants: intra-modality registration and intrapersonal (intra-patient) registration on one side, and inter-modality and interpersonal registration on the other (the registration of measured image data to atlas images or to physical reality in the interventional radiology also belongs here). Registering images may enable better comparison of the image information on the same area provided by different modalities, or by a single modality in the course of time, an assessment of anatomy differences inside a group of patients or volunteers, etc. In these cases, registration itself is the aim of processing, and further derivation of conclusions is left to the medical staff. However, even in this simplest case, fusing information from more images leads to a new quality. Registration may also be the first step of a more complex processing that leads to the automatic narrower-sense *image fusion* serving to derive new images. The simplest and most frequent example is the subtraction of two images (as in the subtractive angiography) in the hope that the difference image would reveal relevant dissimilarities. The preliminary registration is used to prevent enhancing of irrelevant differences due to field-of-view (FOV) shift, differing geometrical distortion, patient movement, etc. The registered images from different modalities may be fused into a single vector-valued image that may serve as a better ground for segmentation or another automatic analysis, or may be presented to the evaluating staff by means such as false colours or overlay techniques.

On the other hand, fusion of single-modality multi-view images covering contiguous parts of an object and overlapping at margins may enable the forming of images of substantially greater FOV. The fusion usually requires both geometrical and gray-scale (or colour)

transforms to enable reasonably seamless joining. The registration in its simplest form finding the best rigid transform, described in three dimensions by only six parameters of shift and rotation is routinely used. However, in many instances, more sophisticated transforms are needed, allowing for compensation of complicated distortions, including multi-view perspective, partial area movement, area shrinking or expanding (possibly space variable), etc. The first step in such cases is to find an appropriate description of the geometrical relations between two (or possibly even more) images. The number of parameters describing a complicated registration transform varies from tens or hundreds of complex flexible formulae to millions in the case of detailed disparity maps. It is obvious that such a parameter set carries information of the relations among the images to be registered (even though no factual registration needed to follow). Thus, the design transform itself may also be considered a fusing operation yielding to output data, otherwise, which may be utilized in the following analysis. In this chapter, we shall follow the standard sequenced steps appearing in image fusion [74, 75, 76, 77, 78, 79, 80, 81, 82, 83, 84, 85, 86, 87, 88, 90]:

- Pre-processing measures, leading in a sense to consistency of involved images, including geometrical transforms and image data interpolation as procedural components,
- Distortion identification via disparity analysis, including description of similarity measures and possibly followed by some wider utilization of disparity maps,
- Proper image registration as a preparatory step for consequent analysis or image fusion,
- Proper image fusion (in the narrower sense) yielding a composite image of a new quality.

IV.2 Brain Tumor's Extraction

IV.2.1 Preprocessing

The low distribution of the gray levels of the original image reduces the contrast of the image. Therefore contrast stretching is employed to increase the dynamic range of the gray levels in the images. The low limit and upper limit for linear contrast stretching are automatically determined from the histogram. Firstly, we construct the histogram of the original image as shown in figure IV.1.(a). From the constructed histogram, it exhibits several peaks. Basically the left peak and the rightmost peak are contributed by the background pixels and the soft tissues respectively. Only the rightmost peak contributed by

the soft tissues consist of useful information. Therefore, we locate the position of the rightmost peak I_p .

In order to obtain a smoother curve, we convolve the histogram in figure IV.1(a) with a vector which each element the value is 10^{-3} . Then, the smoothen curve is transformed into absolute first difference as shown in figure IV.1 (b). From the first difference, the closest peak on the left and right of I_p are auto determined as the lower limit, I_L and the upper limit, I_U respectively for the contrast stretching.

I_L and I_U will then be considered as the input into the linear contrast stretching algorithm as in equation (IV. 1).

$$F(i, j) = I_{max} \frac{(I(i, j) - I_L)}{(I_U - I_L)} \quad (IV. 1)$$

Where I_{max} , $I(i, j)$ and $F(i, j)$ denote the maximum intensity in the image, original image and enhanced image respectively. After the contrast stretching, the obtained result is shown in the Figure IV.2 (b). As can be seen, a much better visualization is obtained [90].

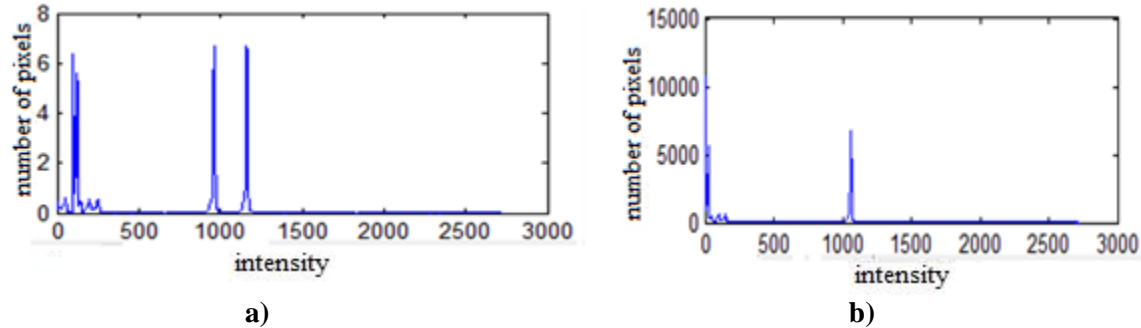


Figure IV. 1. Example of the histogram. **a)** Histogram of a CT brain image, **b)** Histogram of the absolute first difference.

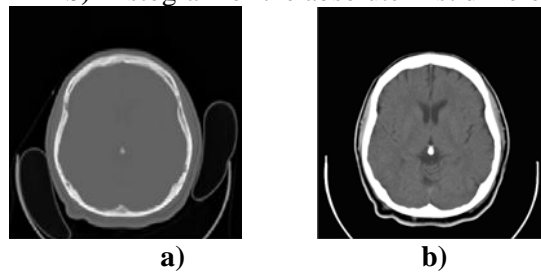


Figure IV. 2. Example of an image before and after enhancement, **a)** Original image, **b)** Enhanced image.

IV.2.2 Post-processing

We have used a Morphological mathematics in post processing step [91, 92, 93].

The morphological transforms were initially applied to images after clustering as a post-processing method helping to remove spurious image elements. It is used to provide elementary analysis of size, shape, and count of objects and to extract the needed information from the different classes obtained such as tumors for abnormal tissue extraction and CSF, gray matter, white matter, bone structure for normal tissue extraction [94].

The basic morphological operators are erosion (\ominus) and dilation (\oplus). Combining them, other operators can be derived, as opening and closing, hit or miss (fit and miss), etc. The operation of all of them is based on using a structuring element, a matrix mask, usually much smaller than the processed image, which is gradually shifted above the image [94].

The mask (structuring element) of a morphological operator is usually binary, but it might acquire gray-level values as well, though it is not utilized in the definitions mentioned below. Obviously, the binary structuring element is a special case of the gray-level mask. We shall limit ourselves to binary masks only. The mask is specified, in addition to by its active set, also by the position of the reference pixel in the mask. The most common size of the mask is 3×3 , but greater masks of possibly anisotropic and irregular shape also may be used. As for the mask content, the two isotropic binary masks, formed by neighboring pixels, are most frequently used. However, greater square, cross, line, or irregularly shaped masks are commonly used as well. In each mask, a cross marks the origin. Composite structuring elements (a couple of non-over-lapping masks) are used. Following both the historical development and a natural way of explanation, we shall present each morphological operator first in its binary form (binary input and output images, binary mask), which will be consequently generalized to the gray-scale type. It should be understood that the binary version is always a special case of the more generic operator. To prevent confusion, we shall formulate the output image g in a new matrix of the same size as the input f , thus preventing any recursion. Furthermore, we shall call the set of active (equal to 1) pixels in a binary image are simply the set of the image [94].

Image morphology provides a way to incorporate neighbourhood and distance information into algorithms (read references [95, 96] for more details in the treatment of morphological operators).

The basic idea in morphology is to convolve an image with a given mask (known as the structuring element), and to binarize the result of the convolution using a given function.

Choices of convolution mask and binarization function depend on the particular morphological operator being used.

Binary morphology has been used in several segmentation systems for providing functional descriptions of morphological as utilised in this work [97].

- **Erosion:** An erosion operation applied on an image I containing labels 0 and 1, with a structuring element S , changes the value of pixel i in I from 1 to 0, if the result of convolving S with I , centred at i , is less than some predetermined value. Let a value is the area of S , which is basically the number of pixels that are 1 in the structuring element itself. The structuring element (also known as the erosion kernel) determines the details of how particular erosion thins boundaries.
- **Dilation** Dual to erosion, a dilation operation on an image I containing labels 0 and 1, with a structuring element S , changes the value of pixel i in I from 0 to 1, if the result of convolving S with I , centred at i , is more than some predetermined value. We have set this value to be zero. The structuring element (also known as the dilation kernel) determines the details of how a particular dilation grows boundaries in an image.
- **Conditional Dilation** A conditional dilation is a dilation operation with the added condition that only pixels that are 1 in a second binary image, I_c , (the image on which the dilation is conditioned), will be turned to 1 by the dilation process. It is equivalent to masking the results of the dilation by the image I_c .
- **Opening** An opening operation consists of erosion followed by dilation with the same structuring element.
- **Closing** A closing operation consists of a dilation followed by erosion with the same structuring element.

Figure IV.3 shows the different steps used for tumor image extraction using morphological operations as post-processing

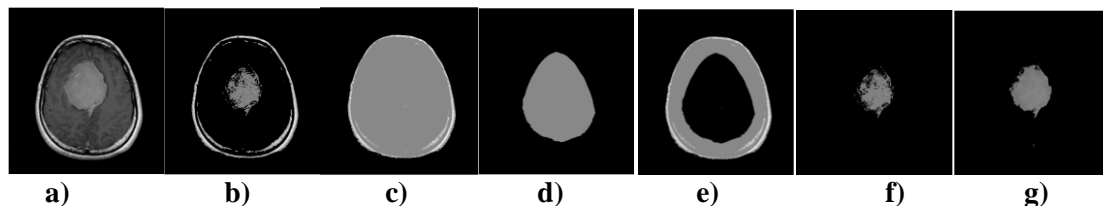


Figure IV.3 shows an example of tumor image extraction using morphological operations.
a) Original image, **b)** Segmented image, **c)** filled holes of **b)**, **d)** erosion applied for **b)**, **e)** ring of **b)**,
f) subtraction of **e)** from **b)**, **g)** filled holes of **f)**.

IV.2.3 Statistics

The main problem is how to get enough data (slices) for the same patient. As an example to calculate the volume for the tumor, we need at least 222 slices which is difficult in deed. So instead of calculating the tumor's volume, calculate the tumor's surface. The algorithm has been applied for many brain scans data, which gives us statistical results. The tumor's surface is calculated as,

$$P_{\%} = \frac{O_{Tu}}{N} * 100 \quad IV.2$$

Where, O_{Tu} is the extracted pixels and N is the total number of the pixels of the image.

IV.3 comparative study of clustering algorithms on Brain Tumor's extraction

The slices used in this study are obtained from the centre of medical imaging "CENTRE DE RADIOLOGIE MAHMOUDI" situated in TIZI-OUZOU. Series of MRI's and CT's slices have been obtained with and without tumors for the same patient, then the different algorithms of clustering have been applied to these images. A number of MRI and CT slices containing the tumor have been taken, then the different clustering algorithms have been applied to them for obtaining the different classes. Finally, the tumor image after post processing using morphological operations listed above has been obtained. After applying algorithm explained previously, all the tumor's normalized surfaces can be calculated (number of tumor's pixel over the total number of the image's pixels) and compared with manual surfaces calculation (which is the method used in many hospitals and clinics in Algeria as MustaphaBacha of Algeria).

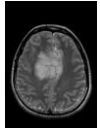





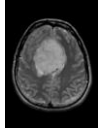





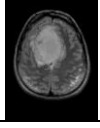





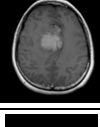





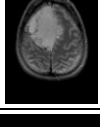



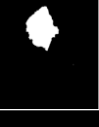

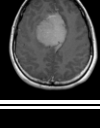



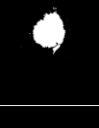

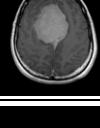


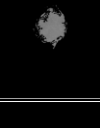


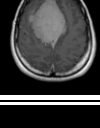





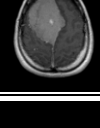





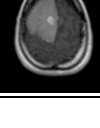





After applying the clustering algorithm to a set of CT and MRI slices, the tumor class has been extracted then post processed. The statistical tumor surface has been calculated then a comparasion between the different algorithms is done.

The table IV.1 shows the results of the post-processing applied to clustering algorithms for tumor extraction. The table IV.2 contains the statistics of the results of tumor image extraction shown in table IV.1.

From the results obtained, we discovered that the EM segmentation gives better results for normal tissue recognition, where the k-means and fuzzy k-means give better results for

abnormal tissue recognition. The thresholding and otsu gives better results for the bone structure (skull) extraction.

Table IV.1: Results of clustering algorithm for tumor image extraction.

Slice number	Slice	Kmeans	Fuzzy kmeans	EM	Threshold	Otsu
1						
2						
3						
4						
5						
6						
7						
8						
9						
10						

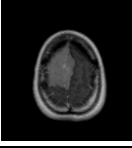






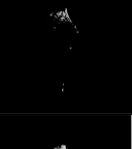


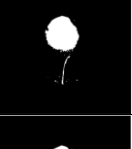

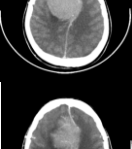
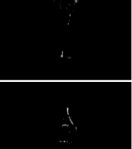

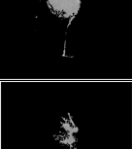
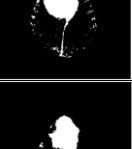

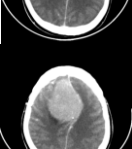

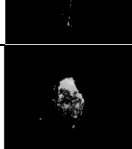
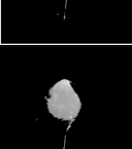
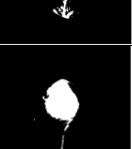

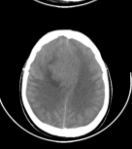
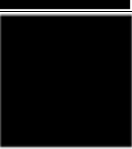




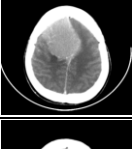
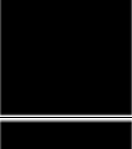

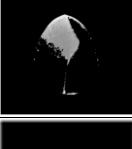


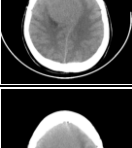





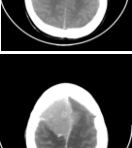

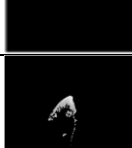

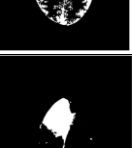
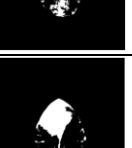












11						
1						
2						
3						
4						
5						
6						
7						
8						
9						

Table IV.2: Statistical efficiency of clustering algorithm for tumor image extraction.

patients	Percentage $P_{\%} = \frac{O_{Tu}}{N} \times 100$	Kmeans	Fuzzy kmeans	EMseg	thresholding	otsu
1	MRI	4.34%	4.31%	1.59%	3.75%	2.76%
2		5.10%	5.16%	4.48%	5.14%	5.12%
3		5.37%	4.84%	4.66%	4.47%	4.66%
4		0.13%	0.20%	1.81%	2.00%	1.49%
5		5.94%	5.85%	5.41%	5.79%	5.60%
6		3.82%	3.81%	3.22%	4.62%	4.01%
7		5.21%	5.40%	3.32%	5.55%	3.75%
8		5.62%	5.69%	5.16%	5.82%	4.02%
9		0.21%	3.60%	C/N/D	1.87%	C/N/D
10		5.30%	5.30%	4.41%	5.60%	C/N/D
11		2.98%	2.37%	3.91%	4.66%	C/N/D
12	CT	0.42%	0.53%	4.15%	4.93%	5.98%
13		1.21%	1.46%	5.51%	7.17%	5.61%
14		0.23%	0.29%	1.64%	5.41%	4.05%
15		3.24%	2.29%	5.90%	5.90%	6.07%
16		C/N/D	C/N/D	C/N/D	2.93%	1.69%
17		C/N/D	1.45%	5.94%	5.83%	6.10%
18		C/N/D	C/N/D	C/N/D	6.56%	4.18%
19		C/N/D	C/N/D	C/N/D	8.69%	5.53%
20		C/N/D	1.49%	4.73%	4.56%	5.43%

C/N/D: Class Not Detected.

IV.4 Proposed Segmentation Method

Most segmentation techniques offer just one level of segmentation to segment all the regions. However, in our approach we adopt the different methods to segment different brain parts. This is due to the some abnormal regions which are too small to form a cluster themselves. The flowchart of the system is shown as in Figure IV.4.

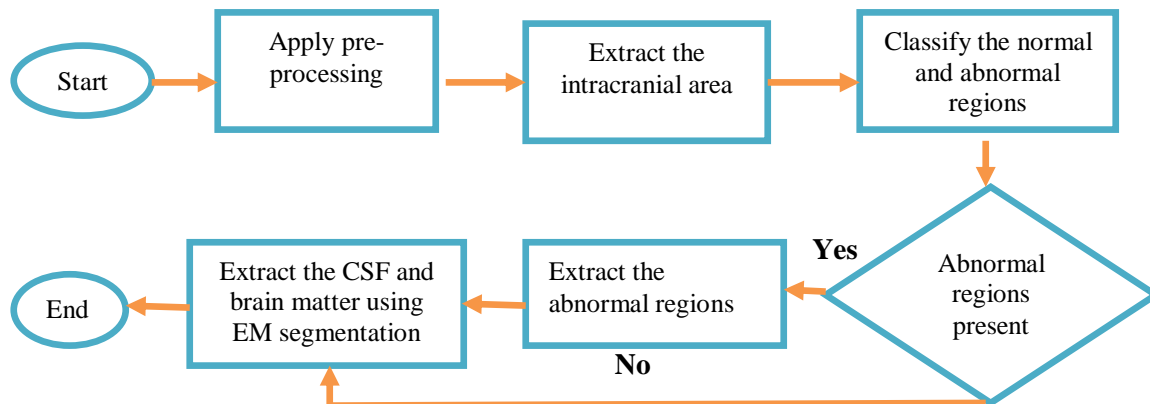


Figure IV.4 Flow chart for the system for segmentation of CT and MRI brain images.

The initial step is to apply the contrast stretching in order to boost the visualization of the original low contrast image. After improvement of the visualization of the image using the post processing, intracranial area is extracted from the contrast stretched image if it is present (sometimes the bone structure is absent in MRI images). In order to extract the intracranial area, we employ thresholding, otsu, and logical operators to the enhanced image. To eliminate the background and skull from the intracranial area, we set the pixel values of the skull and background to zero(black pixel).

For the classification of the image, we experiment on five methods which are k-means clustering, fuzzy k-means (FCM) clustering, expectation-maximization (EM) clustering, threshold and Otsu threshold. It has been observed that two methods which are k-means and FCM clustering can be adopted to identify the potential abnormal regions (tumor in our case). After clustering, a separation of clusters is done. If the abnormal regions are present, we filter out all the abnormal regions before moving on to the next stage. Eventually we apply the EM algorithm to segment the brain CSF and brain matter area from CT images while white matter and gray matter from MRI images.

Figure IV.5 and figure IV.6 show examples of the steps explained on the flowchart of figure IV.4 applied to CT and MRI slices respectively.

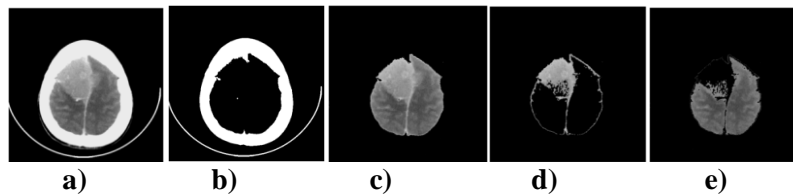


Figure IV.5 extraction of normal and abnormal tissue from CT brain images.

- a) Original CT image, b)the extracted skull, c) the intracranial area, d) the extracted abnormal region, e) the brain matter.

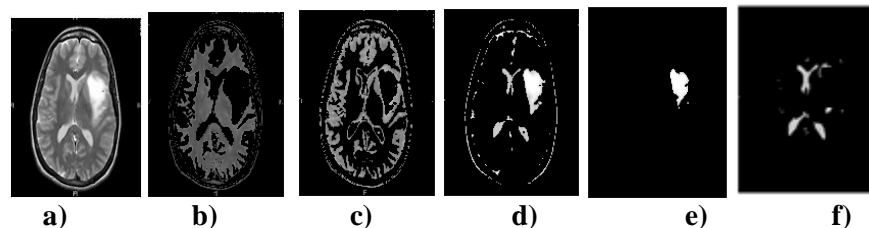


Figure IV.6 extraction of normal and abnormal tissue from MRI brain images.

- b) Original CT image, b)the gray matter area, c) the white matter area, d) the extracted abnormal with CSF region, e) the extracted abnormal region, f) the extracted CSF.

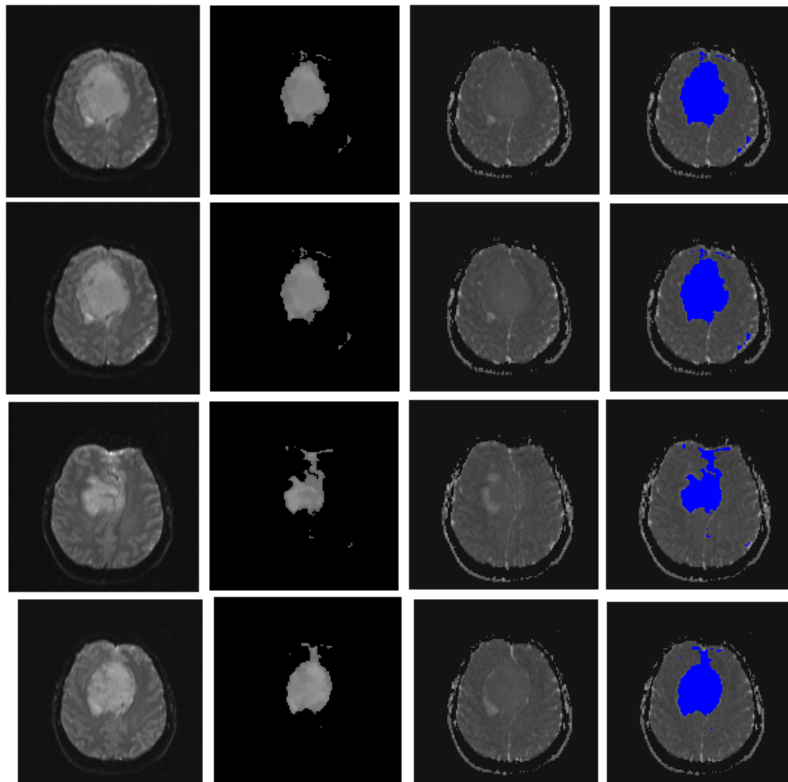
IV.5 Fusion by registration and segmentation

This technique of fusing information from two images can be twofold. The reference image, which is not processed, accommodates a segmented region of interest from the second registered image.

IV.5.1. Monomodal application

An example of this technique is the extraction of the boundary of an object of interest, such as a tumor from the first image and the overlay on the coordinate system of the registered second image of the same modality and of the same patient where the information doesn't appear. Figure bellow shows examples of this case for ct/ct and mri/mri fusion.

First two monomodal images of the same patient are registered, one image contains the tumors where in the second one, the tumor is not clear, next we extracted the tumor using the clustering algorithm and applying post processing depending on the image itself, then we overlay the tumor extracted from the first registered image on the second one using pseudo color map. We applied this method on a set of MRI and CT images, the results are shown in the figure IV.6 and figure IV.7.



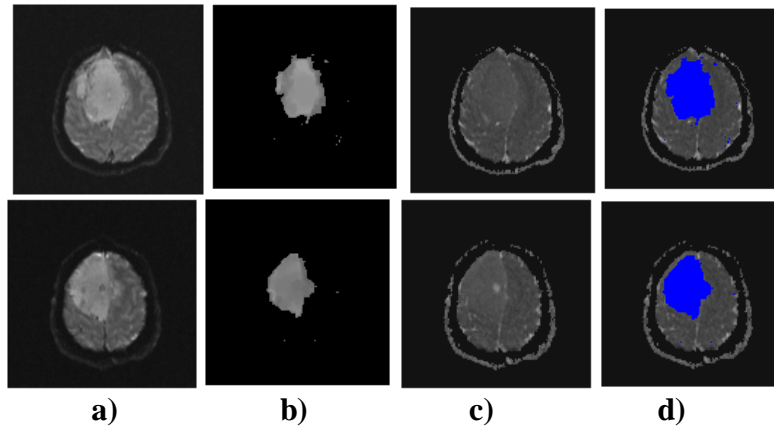


Figure IV.7: extracting tumor from MRI image and overlay it on second MRI image. **a)** registered image, **b)** extracted tumor from the registered image, **c)** original image, **d)** tumor overlaid on the original image.

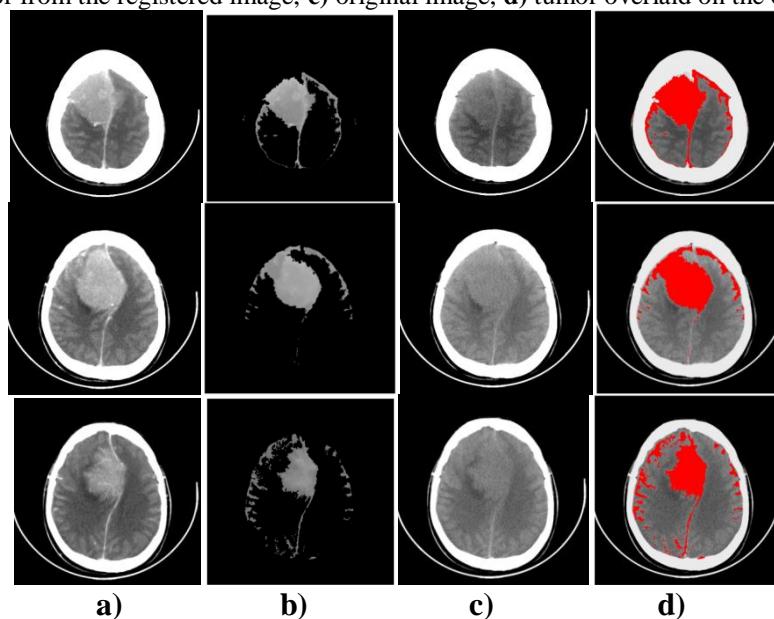
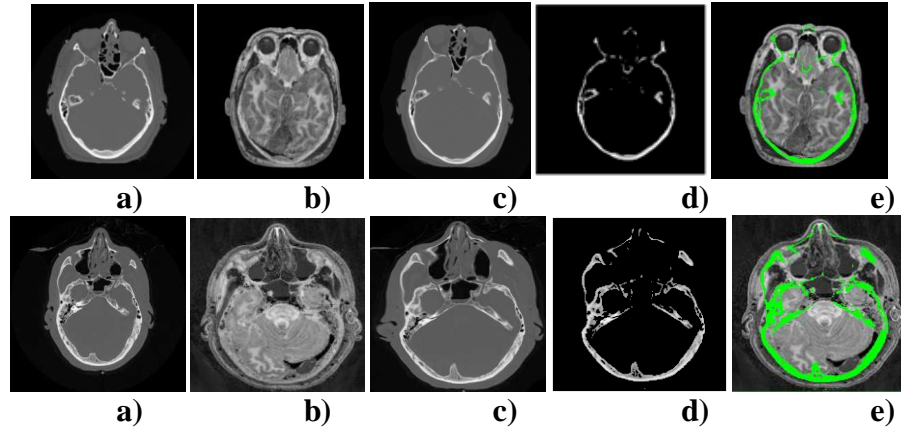


Figure IV.8: Extracting tumor image from CT image and overlay it on second CT image. **a)** registered image, **b)** extracted tumor from the registered image, **c)** original image, **d)** tumor overlaid on the original image.

IV.5.2 Multimodal application

An example of this technique is the extraction of the boundary of an object of interest using the methods given in the previous section, such as a tumor from a MR image and the overlay on the coordinate system of the registered CT image of the same patient.

Fusion technique can be applied using pseudocolormap and clustering algorithm, on multimodal registered CT/MRI images of the same patient, first we apply a registration for the CT image, next we extract the bone structure from the registered CT image, then the extracted bone structure is superimposed on the MRI image where it is overlaid with the green color as shown in the figure IV.9.



FigureIV.9: superposition of bone structure extracted from registered CT on MRI slice.
a) target CT slice, b) reference MRI slice, c) registered CT slice,
d) extracted bone structure from CT slice, e) superposition of (d) on (b).

IV.6 Conclusion

As a conclusion, we have presented our concept for the real CT and MRI brain image fusion. The system performs image registration based on different similarity measures, image segmentation based on different approaches for the different regions of the brain at different stages. The method works effectively for detection of the normal and abnormal regions in the brain and general annotation of the abnormalities can be utilized for the application of the fusion.

Intensity based registration has been used, using coefficient of correlation for monomodal registration and mutual information for multimodal registration. Segmentation has been used to extract information from the registered image to overlay it on the reference image. k-means and fuzzy k-means have been used for normal tissue recognition. EM segmentation has been used for normal tissue recognition. Logical operators, thresholding and otsu have been used for skull extraction. Pseudo colormap has been used in the fusion.

Conclusion

In the recent clinical setting, medical imaging is a vital component in a great number of applications. Such applications are the clinical track of events, not only in clinical diagnosis settings, but prominently so in the area of planning, consumption, and evaluation of surgical and radio-therapeutically procedures.

Medical image fusion is the process that combines information from different images and displays it to the expert as one image, so its diagnostic value is maximized. A first step in this integration process is to bring the modalities involved into spatial alignment, this procedure is named registration. After registration, a fusion step is required for integrating the data involved. By registering the different parts of the body. However, the difficulty is to develop a registration method for monomodal and multimodal images which is suitable to register images containing structures of different rigidities taken from different sensors at different times.

In this work, after describing the brain medical imaging modalities used in medical diagnostic, we have implemented in the first part four types of registration method which are rigid, affine, projective and finally polynomial.

The obtained results are used for registration in monomodal and multimodal applications are described as follows:

- We have implemented intensity based registration and landmark points registration dedicated for recovery of a deformed image. This method is used in neurosurgery, where the original image is completely deformed during the intervention when injecting some solution to the patient needed for the surgery. It is investigated by registration only and it doesn't need the next step of fusion.
- We have applied monomodal and multimodal registration using MRI/CT images of the same patient taken at different times.

In the second part, methods of medical image fusion are described and implemented which are:

- Logical operators method.
- Pseudocolor map method.
- Clustering algorithms for unsupervised fusion of registered images have been used which includes: the k-means algorithm, the fuzzy k-means algorithm, the EM segmentation and finally the threshold algorithm including the Otsu algorithm also have used.

The aim of these methods is to extract a segmented region of interest from the registered image and then overlay it on the second image. This technique of fusion is applied in certain applications in the medical field as discussed in the fourth chapter.

In the third part, we have presented different applications of registration and fusion methods which are summarized below:

- We have made a comparative studies of the clustering methods applied on brain tumor extraction.
- We have performed registration of monomodal images CT/CT and MRI/MRI taken at different times, using the rigid or affine registration depending on the deformation of each couple of images. Then, we have extracted some information from the first image to overlay it on the second image. The extracted data can be from tumor image for monitoring tumor growth, or it can be also a normal tissue (like CSF, WM, and GM) for MRI images. The monomodal fusion aims also to complete an image where the information needed is missed. In the last case, the fusion is of complementary nature.
- We have combined registration/fusion methods and apply it to multimodal images CT/MRI taken from the same patient. The information present in CT (tumor, skull, ...) are absent in MRI, and vice versa. The fused image gives more complete information about the patient.

Finally, we concluded that

Our work is based on MRI/CT images because of the absence of images of the same patient taken at different times for monomodal applications, and different modality of images for the same patient for multimodal applications.

Further Work

We propose for extending and improving this work:

- To use the other methods of registration such as elastic registration.
- To exploit other types of images modality like SPECT and PET and 3-Dimensionality images.
- Enhance the method of post-processing for tumor's extraction.
- Include the specific annotation of the abnormal regions such as hemorrhage, calcification and lesion and their effectiveness in image retrieval application.

References

- [1] Image registration methods: a survey ,Barbara Zitova, Received 9 November 2001; received in revised form 20 June 2003; accepted 26 June 2003.
- [2] An Overview of Medical Image Registration Methods J. B. Antoine Maintz¹ and Max A. Viergever Imaging Science Department, Imaging Center Utrecht, 1998.
- [3] A Survey of Image Registration Techniques Lisa Gottesfeld Brown, Department Of Computer Science, Columbia, University, New York NY10027, January 12, 1992.
- [4] Biomedical Engineering Series, Medical Image Registration Edited by Joseph V. Hajnal Derek L.G. Hill David J. Hawkes, 2001.
- [5] Landmarking and Segmentation of 3D CT Images, Synthesis Lectures on Biomedical Engineering, JohnD. Enderle, University of Connecticut, 2009.
- [6] <http://www.wisegeek.com/what-is-radiology.htm>, visited 13/03/2009
- [7] Biological Psychology, J. W. Kalat, , Brooks/Cole Publishing Company, 5th edition, 1995.
- [8] Principles of Neural Science, E. R. Kandel, J. H. Schwartz, and T. M. Jessell, McGraw-Hill, 4th edition, January 5, 2000
- [9] the Human Brain: An Introduction to Its Functional Anatomy, J. Nolte, C.V. Mosby, 2002.
- [10] <http://www.ncbi.nlm.nih.gov/entrez/query.fcgi?CMD=search&DB=pubmed>
- [11]<http://www.vin.com/VINDBPub/SearchPB/Proceedings/PR05000/PR00159.htm>
- [12] <http://rad.usuhs.mil/index.html>, visited 13/03/2009
- [13] http://www.medicinenet.com/mri_scan/article.htm, visited 13/03/2009
- [14] http://www.medicinenet.com/mri_scan/page2.htm, visited 13/03/2009
- [15] http://neurocog.psy.tufts.edu/images/how_pet_works.gif, visited 13/03/2009
- [16]<http://www.physics.ubc.ca/~mirg/home/tutorial/intro.html>, visited 13/03/2009
- [17] <http://www.physics.ubc.ca/~mirg/home/tutorial/applications.html>, visited 13/03/2009

- [18] Cerebral white matter lesions and subjective cognitive dysfunction, J.C. de Groot, F.-E. de Leeuw, M. Oudkerk, A. Hofman, J. Jolles, and M.M.B. Breteler, 2001.
- [19] Brain facts, a primer on the brain and nervous system. Society for neuroscience, 2008.
- [20] <http://en.wikipedia.org/wiki/Brain>, visited 24/02/2009.
- [21] Handbook of Medical Imaging, Medical Image Processing and Analysis, Chapter 8: Image registration, J.M. Fitzpatrick, D.L.G. Hill and C.R. Maurer, Jacob Beutel (Editor), M. Sonka (Editor), 2009.
- [22] Medical Image Processing, Reconstruction and Restoration, concepts and methods, JIRI JAN, 2006.
- [23] Medical Image Registration: Concepts and Implementation, Jen Mercer, Feb 28, 2006.
- [24] 2-D and 3-D Image Registration for Medical, Remote Sensing, and Industrial Applications. A. Ardeshir Goshtasby, 2005.
- [25] http://en.wikipedia.org/wiki/Image_registration, visited 24/02/2009
- [26] Medical Image Analysis Methods, The Electrical Engineering And Applied Signal Processing Series, Edited by Alexander Poularikas, 2005
- [27] Graphical 3d medical image registration and quantification E.J. Farrell, R.J.T. Gorniak, E.L. Kramer, M.E. Noz, G.Q. Maguire, Jr and D.P. Reddy,. Journal of Medical Systems **2**, 1997.
- [28] Medical Image Registration and Surgery Simulation, Bro-Nielsen, M. PhD thesis, Technical University of Denmark, Department of Mathematical Modelling, 1996.
- [29] Deformations Incorporating Rigid Structures. In Mathematical Methods in Biomedical Image Analysis, Little, J. A., JHill, D. G., and Hawkes, D. J, IEEE Computer Society Press, 1996.
- [30] A Survey of Medical Image Registration J. B. Antoine Maintz_ and Max A. Viergever, Image Sciences Institute, 1998.
- [31] Non-rigid registration using free-form deformations: application to breast MR images, D. Rueckert, L.I. Sonoda, C. Hayes, D.L.G. Hill, M.O. Leach, and D.J. Hawkes, IEEE Trans. Med. Imaging, 1999.
- [32] Predicting error in rigid-body, point based registration, M.J. Fitzpatrick, J. West, and C. Maurer, Jr, IEEE Trans. Med. Imaging, 1998.

- [33] Anatomical-functional correlative analysis of the human brain using three-dimensional imaging systems, A.C. Evans, S. Marret, L. Collins, and T.M. Peters, 1989.
- [34] Accurate frameless registration of MR and CT images of the head: applications in planning surgery and radiation therapy, D.L.G. Hill, D.J. Hawkes, M.J. Gleeson, T.C.S. Cox, A.J. Strong, W.L. Wong, et al, 1994.
- [35] Registration of MR and CT images for skull base surgery using point-like anatomical features, D.L.G. Hill., D.J. Hawkes, J.E. Crossman, M.J. Gleeson, T.C.S. Cox, E.E.C.M.L. Bracey, et al., Br. J. Radiol. 1991.
- [36] Predicting error in rigid-body, pointbased registration, J.M. Fitzpatrick, J. West, and C.R. Maurer, Jr, IEEE Trans. Med. Imaging, 1998.
- [37] The distribution of target registration error in rigid-body, point-based registration, J.B. West and J.M. Fitzpatrick. Proc. Information Processing in Medical Imaging, Springer Lecture Notes in Computer Sciences, 1999.
- [38] Studies in the robustness of multidimensional scaling: perturbational analysis of classical scaling R. Sibson, J.R. Statist, 1979.
- [39] Atlas-Based Fusion of Medical Brain Images, Methods and Applications, Roger Lundqvist, Acta Universitatis Uppsaliensis, Uppsala 2001.
- [40] Alignment by Maximization of Mutual Information, P. Viola and W. M. Wells, 1995.
- [41] Automated Multi-Modality Image Registration based on Information Theory, A. Collignon, F. Macs, D. Delaere, D. Vandermeulen, P. Suetens and G. Marchal, Proc. of Information Processing in Medical Imaging, 1995.
- [42] Multimodality Image Registration by Maximization of Mutual Information F. Macs, A. Collignon, D. Vandermeulen, et al, IEEE Trans. Mcd. Imag, 1997.
- [43] Automated 3D Registration of MR and PET Brairi images by Multiresolution Optimisation of Voxel Similarity Measures, C. Studholme, D. L. G. Hill and D.J. Hawkes, Medical Physics, 1997.
- [44] An Overlap Invariant Entropy Measure of 3D Medical Image Alignment, C. Studholme, D. L. G. Hill and D.J. Hawkes, Patterri Recognition, 1999.
- [45] À Simplex Method for Function Minimization, J. À. Nelder and R. Mead, Coinputer Journal, 1965.
- [46] An Efficient Method of Finding the Minimum of a Function of Several Variables without Calculating Derivatives, M. J. D. Powell, Computer Journal, 1964.
- [47] A general class of nonlinear normalized adaptive filtering algorithms, S. Kalluri and G. R. Arce, IEEE Trans. Signal Processing, 1999.

- [48] A History of the Metropolis-Hastings Algorithm, N. Metropolis et al. Journal of Chemical Physics, 1953.
- [49] A method for optimising the nesting of multiple, highly complex shapes using a modified simulated annealing algorithm, Kirkpatrick, Journal of Statistical Physics, 1984.
- [50] Genetic Algorithms in Search, Optimization, and Machine Learning, D. E. Goldberg, Addison-Wesley, 1989.
- [51] Convergence Properties of the Nelder-Mead Simplex Method in Low Dimensions, Lagarias, J.C., J. A. Reeds, M. H. Wright, and P. E. Wright, SIAM Journal of Optimization, 1998.
- [52] en.wikipedia.org/wiki/Image_fusion, visited 07/06/2010.
- [53] Medical Image Registration and Fusion Techniques: A Review, Matsopoulos, George K. et al, 2001.
- [54] Warping and Morphing of Graphical Objects, J. Gomes, L. Darsa, B. Costa, and L. Velho, Morgan Kaufman Publishers, 1998.
- [55] Algorithms for Clustering Data, A. K. Jain and R. C. Dubes, , Prentice-Hall, Englewood Cliffs, 1988.
- [56] http://en.wikipedia.org/wiki/K-means_algorithm, visited 07/06/2010.
- [57] Segmentation of MR images by a fuzzy C-means algorithm, R. Rezaee, C. Nyqvist, P. van der Zwet, E. Jansen, and J. Reiber, Comput. Cardiol, 1995.
- [58] http://en.wikipedia.org/wiki/Cluster_analysis, visited 07/06/2010.
- [59] <http://www.cs.ualberta.ca/~nray1/CMPUT615/K-meansClustering.ppt>, 07/06/2010.
- [60] An Efficient k-Means Clustering Algorithm: Analysis and Implementation, Tapas Kanungo, Senior Member, David M. Mount, Member, Nathan S. Netanyahu, Member, Christine D. Piatko, Ruth Silverman, and Angela Y. Wu, Senior Member, IEEE, 2002.
- [61] K-means and Hierarchical Clustering, Andrew W. Moore Associate Professor School of Computer Science Carnegie Mellon University, 2001.
- [62] Pattern Recognition with Fuzzy Objective Function Algorithms, Bezdek, J. C, 1981.
- [63] Partition structures: a tutorial, in The Analysis of Fuzzy Information, Boca Raton, J. Bezdek, 1987.
- [64] rss.acs.unt.edu/Rdoc/library/e1071/html/cmeans.html, visited 07/06/2010.
- [65] cwiki.apache.org/MAHOUT/fuzzy-k-means.html, visited 07/06/2010.

- [66] The representation of grammatical categories in the brain, Kevin Shapiro and Alfonso Caramazza, Harvard University, 2003.
- [67] <http://en.wikipedia.org/wiki/Thresholding>, visited 07/06/2010.
- [68] Thresholding, c Bryan S. Morse, Brigham Young University, 1998–2000.
- [69] Thresholding. In Digital Image Processing, Gonzalez, Rafael C. & Woods, Richard E, 2002.
- [70] http://en.wikipedia.org/wiki/Otsu's_method, visited 07/06/2010.
- [71] Tutorial on Expectation-Maximization: Application to Segmentation of Brain MRI, Maria Murgasova, 2007.
- [72] Normalized Cuts and Image Segmentation, Jianbo Shi & Jitendra Malik, IEEE Conf. Computer Vision and Pattern Recognition 1997.
- [73] Image Segmentation using k-means clustering, EM and Normalized Cuts, Suman Tatiraju, Avi Mehta, Department of EECS University Of California, 2009
- [74] Image registration. In Handbook of Medical Imaging, Medical Image Processing and Analysis, Fitzpatrick, J.M., Hill, D.L.G., and Maurer, C.R., Jr. Sonka, SPIE, International Society for Optical Engineering, 2000.
- [75] Medical Image Registration, Hajnal, J.V., Hill, D.L.G., and Hawkes, D.J. (Eds.) CRC Press, Boca Raton, FL, 2001.
- [76] Digital Image Processing, Gonzalez, R.C. and Woods, R.E.. Addison-Wesley, Reading, 1992.
- [77] Stereo Terrain Reconstruction By Dynamic Programming In Handbook of Computer Vision and Applications, Gimel'farb, G. Jahne, B., Haussecker, H., Geissler, P. (Eds.), 1999.
- [78] Motion. In Handbook of Computer Vision and Applications, Vol. 2, Jahne, B., Haussecker, H., Geissler, P. (Eds.). 1999.
- [79] Complex Approach To Surface Reconstruction Of Microscopic Samples From Bimodal Image Stereo Data, Jan, J. and Janova, D. Mach. 2001.
- [80] Two-Dimensional Non-Linear Matched Filters, Jan, J, Paper presented at Proceedings of 2nd International Conference, Bratislava, Slovakia, 1996.
- [81] Optimization Methods For Registration Of Multimodal Images Of Retina, Kubecka, L., Skokan, M., and Jan, J. In Proceedings of 25th Annual International Conference of IEEE-EMBS, 2003.

- [82] Stereoscopic Image Processing, In The Digital Signal Processing Handbook., Lagendijk, R.L., Franich, R.E.H., and Hendriks, E.A. Madisetti, V.K., Williams, D.B. CRC Press/IEEE 1998.
- [83] Principles For Automatic Scale Selection, In Handbook of Computer, Vision and Applications, Lindeberg, T. Jahne, B., Haussecker, H., Geissler, P, 1999.
- [84] SEGMENTATION and Registration of Multimodal Medical Images, Maes, F. Ph.D. dissertation, Katholieke Universiteit Leuven, Belgium, 1998.
- [85] Digital Image Processing, Pratt, W.K, John Wiley & Sons, New York, 2001.
- [86] Geometrical And Global Aspects, In Handbook of Computer Vision and Applications, Mallot, H.A. Stereopsis, Jahne, B., Haussecker, H., Geissler, P, New York, 1999.
- [87] The Color Image Processing Handbook, Sangwine, S.J. and Horne, R.E.N, Chapman & Hall, New York, 1998.
- [88] Registration Of Multimodal Images Of Retina, Skokan, M., Skoupy, A., and Jan, J, In Proceedings of 24th Annual International Conference of IEEE-EMBS, Houston, 2002.
- [89] Methods for Registration, Interpolation and Interpretation of Three-Dimensional Medical Image Data for Use in Three-Dimensional Display, Three-Dimensional Modelling and Therapy Planning, Vandermeulen, D. Ph.D. dissertation, Katholieke Universiteit Leuven, Belgium, 1991.
- [90] Segmentation of CT Brain Images Using Unsupervised Clusterings, Tong Hau Lee, Mohammad Faiza Ahmad Fauzi and Ryoichi Komiya, 2009.
- [91] Image Analysis and Mathematical Morphology, J. Serra , London; New york, 1982.
- [92] Living Anatomy, R. A. Novelline and L. F. Squire, Hanley and Belfus, 1987.
- [93] Characterization of normal brain tissue using seven calculated MRI parameters and a statistical analysis system, T. J. Hyman, R. J. Kurland , G. C. Leavy and J. D. Shoop, Magnetic resonance in medicine, 1989.
- [94] Medical image processing reconstruction and restoration, concepts and methods, Jiri Jan, Taylor & Francis, 2006.
- [95] Image Analysis and Mathematical Morphology, J. Serra.. London Academic, 1982.
- [96] Image analysis using mathematical morphology, R.M. Haralick, S.R. Sternberg, and X. Zhuang.. IEEE Transactions PAMI, 1987.

References

[97] Segmentation of Brain Tissue from Magnetic Resonance Images, Tina Kapur, Massachusetts Institute Of Technology Artificial Intelligence Laboratory, 1995.

[98] Pattern Recognition with Fuzzy Objective Function Algorithms, Bezdek, James C, 1981.

[99] Automatic Assessment Method For CT-MR Image Fusion Based On A Local Confidence Measure, Puja Malik, Ion Pappas, Jubei Liu, Martin Styner, and Marco Caversaccio M.E.Müller Research Center, Institute of Surgical Technology and Biomechanics, University of Bern.

[100] Multilevel Medical Image Fusion using Segmented Image by Level Set evolution with Region Competition, Shruti Garg, K. Ushah Kiran, Ram Mohan, U S iway, Proceedings of the 27 th Annual International Conference of IEEE EMBS, 1-4 Sept. 2005, Sanghai, China.

[101] PET-MRI Image Registration And Fusion Using Artificial Neural Networks Woei-Fuh Wang¹, Frank Qh Ngo¹, Jyh-Cheng Chen¹, Ray-Ming Huang¹, Kuo-Liang Chou², And Ren-Shyan Liu², 2003.